(2)

EXPERIMENTAL INVESTIGATIONS OF TRANSPORT AND OPTICAL PROPERTIES OF III-V QUANTUM WELL STRUCTURES GROWN VIA MOLECULAR BEAM EPITAXY UNDER OPTIMAL GROWTH CONDITIONS

FINAL REPORT

JUNE 1990

ARMY RESEARCH OFFICE
RESEARCH TRIANGLE PARK
P.O.BOX 12211
NORTH CAROLINA, 27709-2211

CONTRACT # DAAL 03-86-K-0102

PERIOD COVERED: JUNE 13, 1986 - JUNE 12, 1989

A. MADHUKAR
UNIVERSITY OF SOUTHERN CALIFORNIA
LOS ANGELES, CA 90089-0241

APPROVED FOR PUBLIC RELEASE;

DISTRIBUTION UNLIMITED

REPORT DOCUMENTATION PAGE

Form Approved
OMB No. 0704-0188

1. AGENCY USE ONLY (Leave blank)	2. REPORT DATE	3. REPORT TYPE AND DATES COVERED
		FINAL REPORT 6/13/86-10/15/1989

4. TITLE AND SUBTITLE
EXPERIMENTAL INVESTIGATIONS OF TRANSPORT AND OPTICAL PROPERTIES OF III-V QUANTUM WELL STRUCTURES GROWN VIA MOLECULAR BEAM EPITAXY UNDER OPTIMAL GROWTH CONDITIONS.

5. FUNDING NUMBERS
DAAL 03-86-K-0102

6. AUTHOR(S)
A. MADHUKAR

7. PERFORMING ORGANIZATION NAME(S) AND ADDRESS(ES)
UNIVERSITY OF SOUTHERN CALIFORNIA
SCHOOL OF ENGINEERING
DEPARTMENT OF MATERIALS SCIENCE VHE 506
LOS ANGELES, CA 90089-0241

8. PERFORMING ORGANIZATION REPORT NUMBER

9. SPONSORING/MONITORING AGENCY NAME(S) AND ADDRESS(ES)
U. S. Army Research Office
P. O. Box 12211
Research Triangle Park, NC 27709-2211

10. SPONSORING/MONITORING AGENCY REPORT NUMBER
ARO 23726.22-EL

11. SUPPLEMENTARY NOTES
The view, opinions and/or findings contained in this report are those of the author(s) and should not be construed as an official Department of the Army position, policy, or decision, unless so designated by other documentation.

12a. DISTRIBUTION/AVAILABILITY STATEMENT
Approved for public release; distribution unlimited.

12b. DISTRIBUTION CODE

13. ABSTRACT *(Maximum 200 words)*

A series of experimental studies have been conducted to explore; (1) the optimization of transport and optical properties of quantum structures via control of the growth kinetics during molecular beam epitaxy and (2) relation of these properties with the structure design. As a result of a combined approach of material science, physics, and device engineering research, quantum structures with the best properties to-date, such as the resonant tunnelling diodes with high peak to valley ratio and large peak current density, inverted heterojunction structures with ultra-low density and high mobility suitable for the basic study of quantum Wigner solid states, etc., have been grown. Carrier scattering induced by interface roughening and interface trapped impurity and exciton scattering induced by band edge discontinuity fluctuations and alloy disorder have been demonstrated. A strong phenomenon of double resonant Raman scattering and optical phonon-electron resonance mixing is observed in specially designed structures. The possibility of in-situ fabrication of laterally confined nano-structures via growth on pre-patterned substrates has been explored. Additionally, benefits of using external beams to control the growth kinetics have been investigated. All these results are helpful towards a better understanding of the nature of quantum structures. They also provide a strong basis for the design and fabrication of some novel device structures in the future.

14. SUBJECT TERMS	15. NUMBER OF PAGES
QUANTUM WELL STRUCTURES, MOLECULAR BEAM EPITAXY, REFLECTION ELECTRON DIFFRACTION, OPTIMIZED GROWTH KINETICS, INVERTED HEMT, PATTERNED SUBSTRATE GROWTH, IN SITU FABRICATION OF LATERALLY CONFINED STRUCTURES, STRAINED EPITAXY	66
	16. PRICE CODE

17. SECURITY CLASSIFICATION OF REPORT	18. SECURITY CLASSIFICATION OF THIS PAGE	19. SECURITY CLASSIFICATION OF ABSTRACT	20. LIMITATION OF ABSTRACT
UNCLASSIFIED	UNCLASSIFIED	UNCLASSIFIED	UL

TABLE OF CONTENTS

PREAMBLE:

These pages contain the Final Scientific Report on the work accomplished and various activities undertaken under Contract No. DAAL 03-86-K-0102. Section I of the report covers work accomplished and is divided into two main subsections covering transport and optical studies, respectively. Section II provides a list of publications either solely or partially supported by this contract, section III a list of personnel, and section IV a brief description of collaborative interactions.

I. WORK ACCOMPLISHED:

In this section we provide a brief description of some of the salient accomplishments. The work accomplished is grouped under different headings which are indicative of the generic theme.

(I.1) PARALLEL TRANSPORT

(I.1.A) TRANSPORT IN HETEROJUNCTIONS AND SQUARE QUANTUM WELLS:

During the period June '86 - Jan. '88 we focussed on certain outstanding experimental and theoretical issues relating to electron transport parallel to the interfaces in heterojunctions (HJ's) and square quantum wells (SQW's). In the former category we focussed on the inverted high electron mobility transistor (I-HEMT) whereas, in the latter category, we focussed on the single SQW.

THE I-HEMT

Through usage of the growth and surface smoothness recovery kinetics of GaAs(100) and $Al_xGa_{1-x}As$(100) growth fronts extracted from our RHEED studies during MBE, we arrived at an optimized approach to growing I-HEMT structures which would maintain high quality inverted interface in spite of usage of very low (500-550°C) growth temperature during modulation doping of $Al_{0.25}Ga_{0.75}As$. The notion of growth interruption was employed with the novel twist of delivering $\leq$ 1 ML of GaAs periodically during $Al_{0.25}Ga_{0.75}As$ growth prior to growth interruption. Comparison of the inverted HEMT's grown (during 1986) on our Φ-400 MBE machine following conventional approach and our new approach showed an increase in mobility by a factor of 5 to 7 but the absolute values were still limited to ~ 22,000 cm^2/V-sec. This was clearly attributable to the lack of adequate background vacuum conditions of this old machine as revealed by high carbon and other impurity related luminescence. The correctness of the basic idea being, however, demonstrated by the results, we initiated a collaboration with colleagues at the US Army Electronics and Device Technology Laboratory, Ft. Monmouth, to grow the I-HEMT structures following our approach on their high quality Varian GenII MBE machine. The very first set of I-HEMT grown showed LN_2 mobilities in the dark between 80,000 and 90,000 cm^2/V-sec for carrier concentrations of ~ 5-7x10^{11}/cm^2. Mobilities under light were as high as ~ 125,000cm^2/V-sec. These remarkably high mobilities (a factor of 5 better than those previously reported without the use of superlattice buffer layers) established the correctness of the ideas and demonstrated, for the first time, that I-HEMT mobilities can be made comparable to the normal HEMT's. Further details may be found in **publications nos. 9,10 and 11** of the publication list given in sec. II.

SINGLE SQUARE QUANTUM WELL:

In parallel with the I-HEMT effort noted above, we undertook both theoretical and experimental work on the behavior of electron mobility in single square quantum well (SSQW) of $GaAs/Al_{0.3}Ga_{0.7}As$ as a function of well width (d_w), spacer layer thickness (d_{sp}), single side modulation doping (inverted and normal) and carrier concentration. We developed self-consistent solutions for coupled Schrodinger and Poisson equations accounting for the electron-electron exchange and correlation effects within the $X\alpha$ approximation. The resulting self-consistent bound state energies, wave functions, and charge density distribution were employed to examine the role of remote ionized impurity, alloy disorder and band edge discontinuity fluctuation induced scattering employing the memory function approach based on the Kubo formalism. The results showed that the low temperature mobilities in ~200A wide wells can be as high as 4 to 5 $x10^6$ cm^2/V-sec, though for normal side modulation doped SSQW this is about a factor of 2 smaller than the highest mobilities possible in N-HEMT. A number of other interesting predictions also came out of these calculations, discussed in **publication nos. 4 and 5.**

On the experimental side a large number of SSQW's were grown with varying structural and/or doping schemes, including δ-doping. Their Hall mobility behavior was systematically examined as a function of temperature (4K to 300K). The predicted factor of 2 difference between the N-HEMT and SSQW was confirmed although the absolute value for the latter was limited to 52,000 cm^2/V-sec at LN_2 temperature. This was directly attributable to the less than necessary ambient quality of our Φ-400 MBE machine and we have no doubt that, just as in the case of I-HEMT discussed above, growth in high quality machines is fully capable of improving the SSQW mobilities by at least the same factor of 5 as found for

(a) NORMAL STRUCTURE

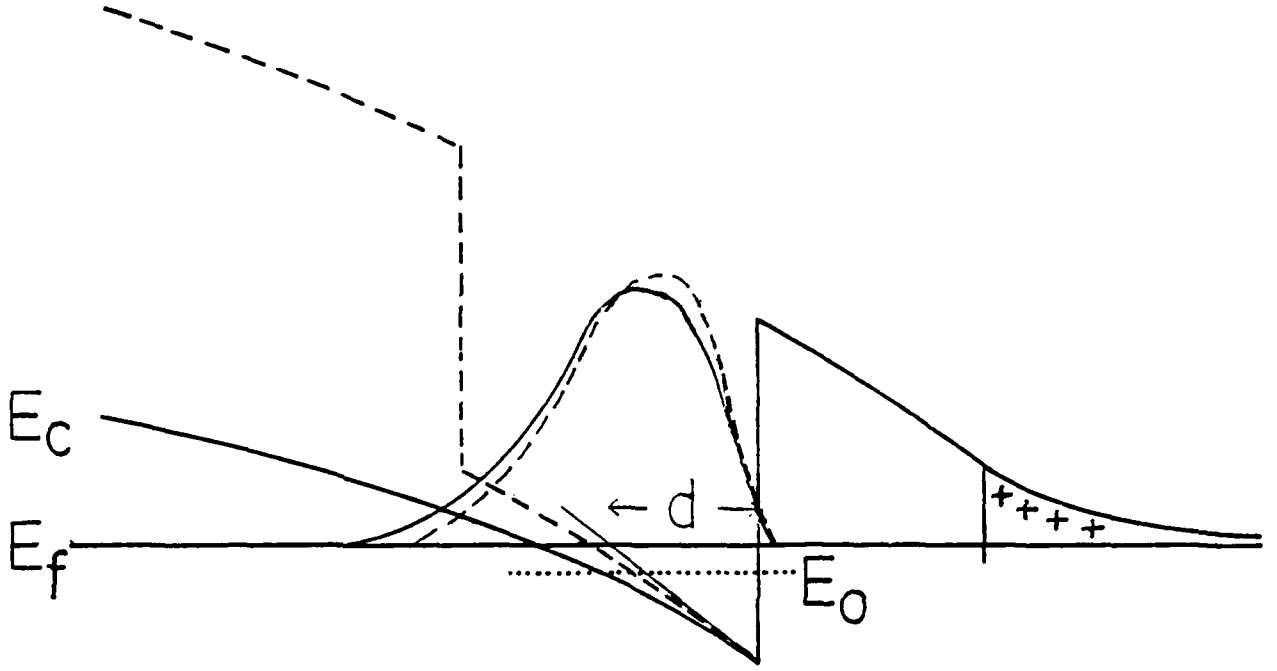

surface →

(b) INVERTED STRUCTURE

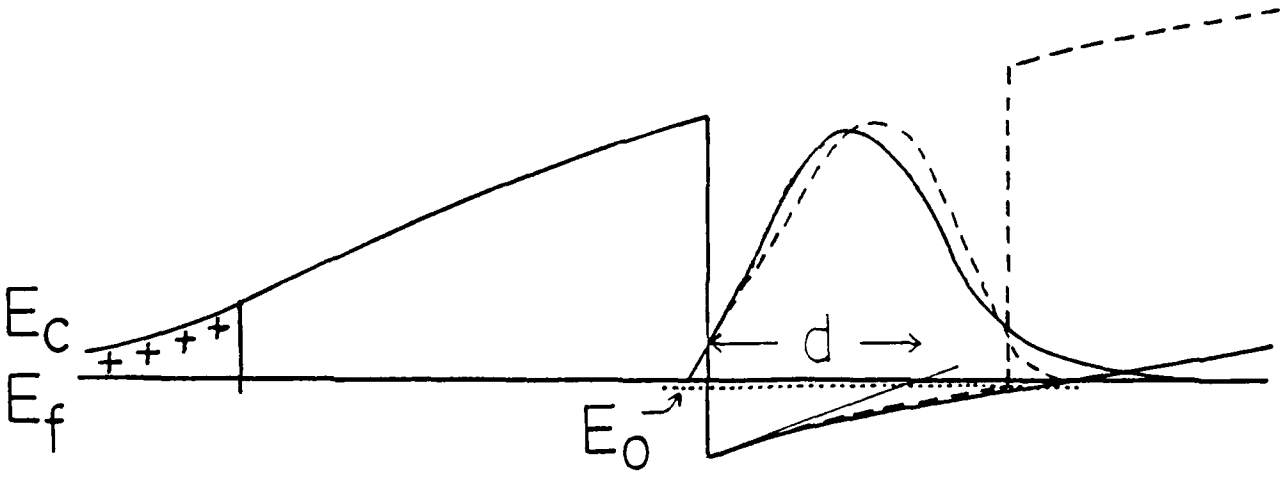

Fig. 1

I-HEMT's, if not even more.

A very interesting result which has emerged from the studies so far is the first unambiguous identification of the influence of the inverted interface induced scattering in SSQW. We note here the salient findings. Introduction of a square well in the normal HJ was found to decrease the mobility by a factor of two whereas for the inverted structure the mobility was found to increase by a factor of two. This unexpected latter result is shown to be a consequence of the shifting of the confined carrier charge distribution away from the inverted interface due to a self-consistent change in band bending as schematically represented in fig. 1 (panel (a) for the normal and panel (b) for the inverted structure). This has led to the recognition that in an inverted structure the absolute mobility of the SSQW can be even higher than the I-HEMT if one is already in the regime where the I-HEMT mobility is limited by the inverted interface scattering rather than remote ion scattering. This is not possible in the normal structure, thus indicating that the I-SSQW (and not I-HEMT) can have mobilities as high as the N-HEMT. Further details may be found in the Ph.D disseratation of Dr. Do-Jin Kim (University of Southern California, 1989.

(I.1.B) ULTRA LOW DENSITY, HIGH MOBILITY INVERTED STRUCTURES:

Since our new RIBER 3200P MBE system was delivered and became operational in Fall 1988, we have succeeded in obtaining unheard of LN_2 dark mobilities of 145,000 to 180,000 $cm^2/V\text{-}sec$ in I-HEMT structures with the remarkably low electron density of $\sim 3\text{-}4 \times 10^{10}/cm^2$ (see publication number 18). Although such low density electron gas is of no particular significance to any conventional electronic device, the greater achievement here is the realization of such high mobilities at such low densities - a much sought after objective

for basic Physics studies and one at which previous attempts by many have been unsuccessful. Such electron gases are suited for both examination of transport and magneto-transport characteristics in a regime of electron density previously not available (along with high mobility) and possible examination of new electron-electron interaction dominated phenomenon at very low temperatures ($\leq$ 100 mK) and very high magnetic fields ($\geq$ 15T). This regime includes such things as charge density wave and possibly quantum Wigner solid formation, apart from the integral and fractional quantum Hall effects. We summarize in this subsection our findings on the scattering mechanisms in the ultra low density regime, the results on the magneto-transport being summarized in the next subsection.

An illustrative example of the temperature dependence of the dark mobility and carrier density of an I-HEMT made from wafer no. RG890213 and obtained using Hall bar geometry is shown in fig. 2(a). The LN_2 mobility is already a remarkably high value of ~1.6×10^5 cm^2/V-sec at the ultra-low carrier density (n) of $4\times10^{10}/cm^2$. While n remains constant at lower temperatures, the mobility rises but saturates at ~ $4\times10/cm^2$/V-sec below about 10K. The carrier density dependence at 300K, 77K, and 4.2K is shown in fig. 2(b), along with the value of the slope α in the relation $\mu \sim n^{\alpha}$. The low temperature slope of 0.7 to 0.8 rules out mobility limited by remote ionized impurity scattering and background impurity scattering as these are theoretically predicted to give α between 1.0 and 1.5 for the former and between 0.5 and 0.6 for the latter. The very high value of mobility at 77K and the very weak temperature dependence at lower temperatures, combined with the maximum in μ occurring at a low n of ~ $1\times10^{11}/cm^2$ in fig. 2(b) (usually the maximum in μ is observed for n ~5-$8\times10^{11}/cm^2$ and has been attributed to the onset of inter subband scattering) suggested to us that the maximum in μ in these I-HEMT's is likely due to the interplay between interface

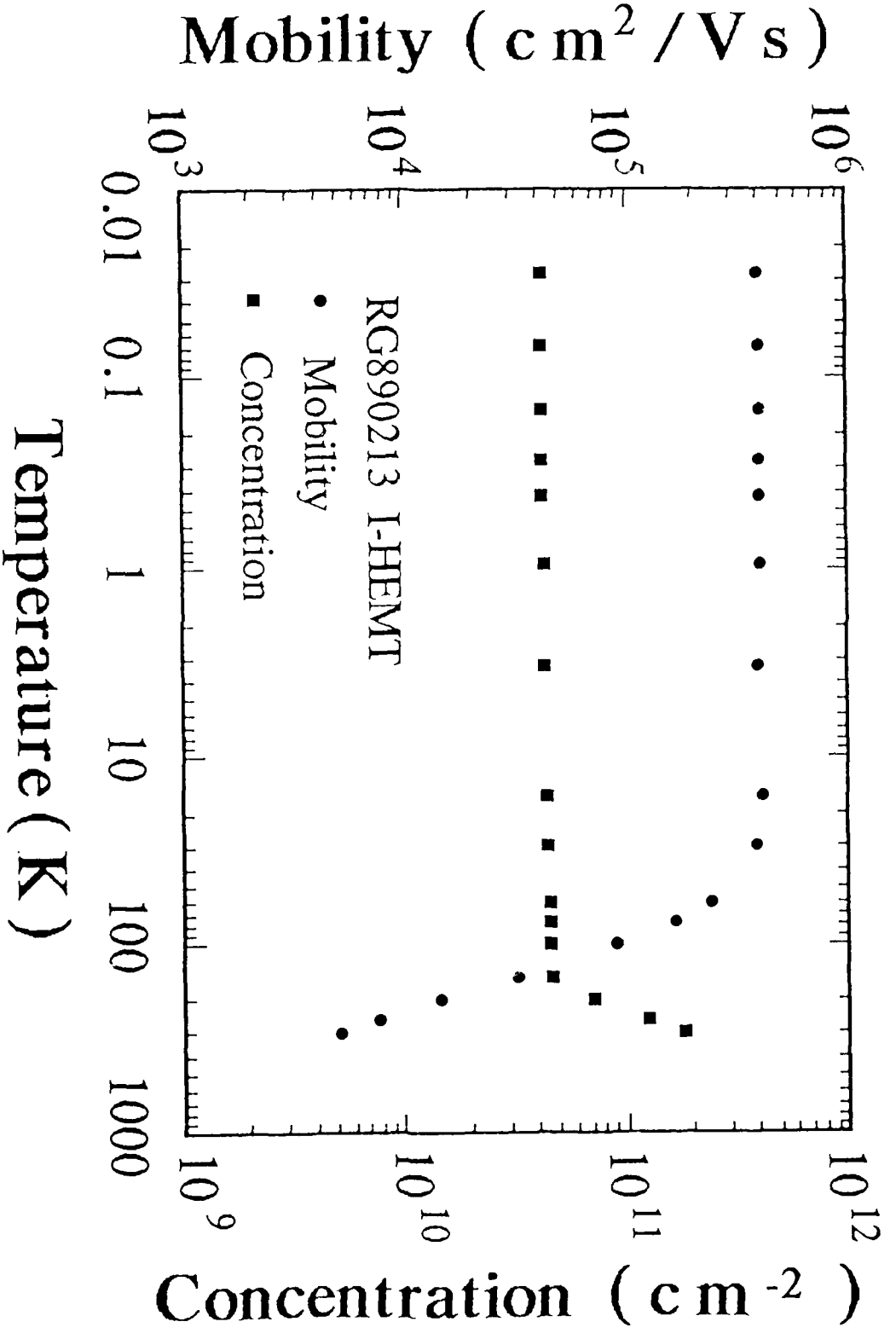
Mobility (c m^2 / V s)
10^3
10^4
10^5
10^6
0.01
0.1
1
10
100
1000
Temperature (K)
RG890213 I-HEMT
Mobility
Concentration
10^9
10^{10}
10^{11}
10^{12}
Concentration (c m^{-2})

Fig. 2(a)

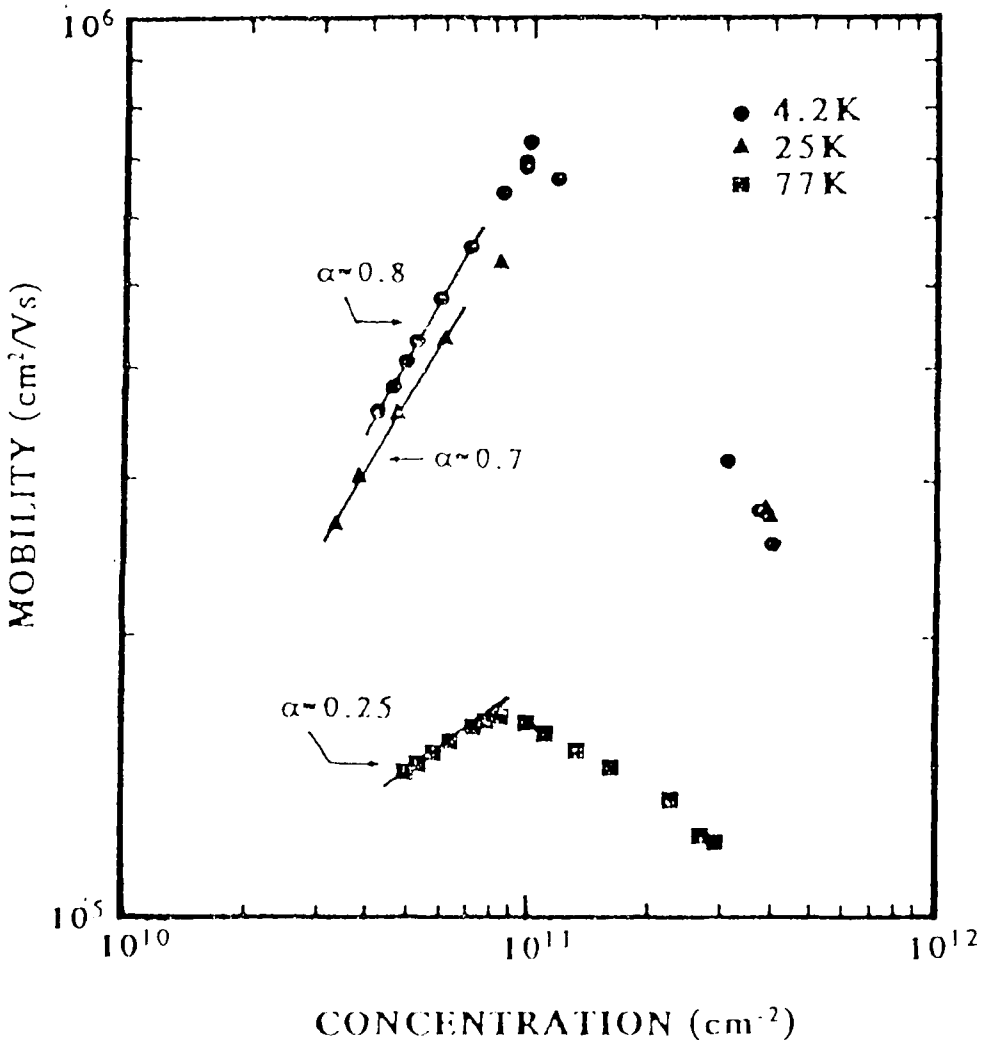

Fig. 2(b). Electron mobility of inverted heterojunction sample No. 890213-01-A at 77, 25, and 4.2 K as a function of sheet electron concentration. Solid lines indicate the relation $\mu \propto n^{\alpha}$, with $\alpha \approx 0.25$, 0.7, and 0.8, respectively.

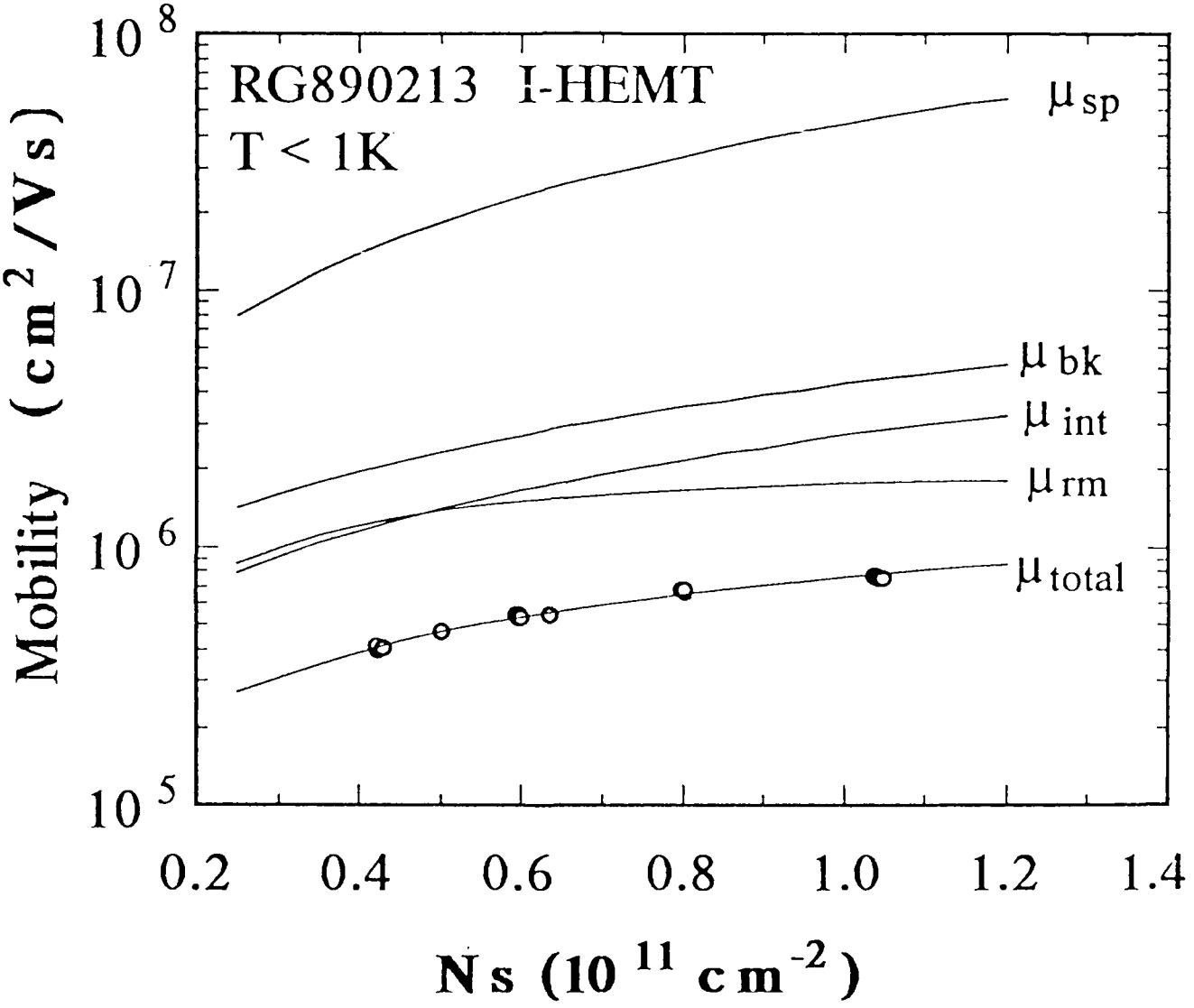
RG890213 I-HEMT
T < 1K
μsp
μbk
μint
μrm
μtotal
Mobility (cm²/Vs)
10⁸
10⁷
10⁶
10⁵
0.2
0.4
0.6
0.8
1.0
1.2
1.4
Ns (10¹¹ cm⁻²)

Fig. 3

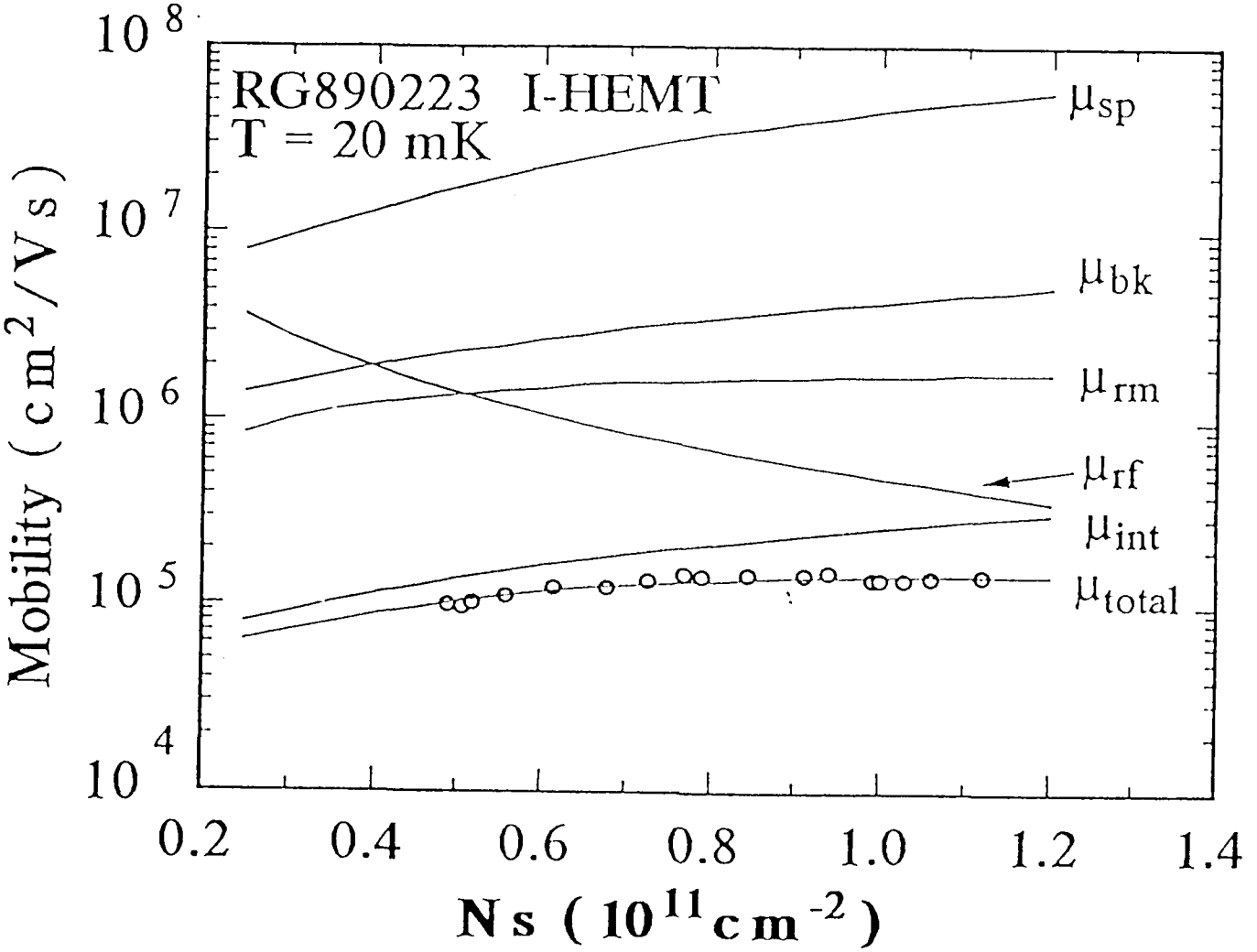
RG890223 I-HEMT
T = 20 mK
μ_{sp}
μ_{bk}
μ_{rm}
μ_{rf}
μ_{int}
μ_{total}
Mobility (cm^2/Vs)
10^8
10^7
10^6
10^5
10^4
0.2
0.4
0.6
0.8
1.0
1.2
1.4
Ns ($10^{11} cm^{-2}$)

Fig. 4

trapped impurity scattering and interface roughness scattering.

To ascertain this new feature, we examined the μ vs. n behavior at ultra-low temperatures (20mK to 4.2K), undertook self-consistent calculations of the electronic structure, and calculated electron scattering due to background impurities (in GaAs and AlGaAs), remote ionized impurity scattering, interface roughness, and, for the first time, interface trapped impurity scattering. The data and the obtained best theoretical fit for the I-HEMT sample of fig.2 and for a 200A inverted square quantum well (I-SQW) are shown in figures 3 and 4, respectively. To obtain the fit the I-HEMT did not require any interface roughness scattering but required an interface trapped charge density of only $1x10^9/cm^2$. The I-SQW on the other hand required a root mean square interface roughness amplitude of 4.9A with a lateral correlation length of ~ 50A and interface trapped impurity density of ~ $5x10^9/cm^2$, consistent with its lower mobility. Details may be found **in publications 18 and 19.**

(I.1.C). INTEGRAL AND FRACTIONAL QUANTUM HALL EFFECT IN INVERTED STRUCTURES:

In the absence of a random potential (such as arising from interface roughness, impurities, etc.) an ideal quasi two dimensional electron gas (2 DEG) subjected to a magnetic field is predicted to undergo two types of ground states as a function of decreasing Landau level filling factor, $\nu=(nh/eB)$ where n is the ideal 2D density of states. These are the fractional quantum Hall effect states occurring for $\nu=(p/q)<1$ where p and q are integers and the quantum Wigner solid (QWS) state, both a consequence of the electron-electron Coulomb repulsion, $U\sim(e^2/\varepsilon a)$ in which ε is the dielectric constant of the medium within which the 2D electron system resides and a is the QWS lattice constant, inversely pro-portional to the square

root of the electron density ($a \sim n^{-1/2}$). With decreasing (i.e. increasing B field and a fixed n) at sufficiently low temperatures the system goes through various FQHE states and, at zero Kelvin, a first order phase transition is predicted to occur as the system goes from a correlated quantum fluid state manifest in the FQHE to an electron solid state characterized by rigidity of the collective electron system. A melting transition is thus predicted to occur in the QWS state with increasing temperature. The FQHE states, by contrast, are not expected to exhibit a phase transition but only a gradual weakening of the correlated quantum fluid nature with increasing thermal energy.

All real systems invariably have a certain degree of random potential arising from the sources noted above. The presence of such disorder potential gives rise to magnetic field dependent energy regions of Anderson localized single quasi particle states whose consequence is believed to be manifest in the integral quantum Hall effect (IQHE), observed as plateaus in ρ_{xy} occurring at (e^2/hi) for i=integer and the corresponding minima in ρ_{xx}. The relative strengths of the disorder potential $e\langle V_D \rangle$ and the Coulomb repulsion U thus become of utmost significance in a real system in controlling the nature of the electron system quantum states accessible as a function of increasing magnetic field. It is to be explicitly recognized that in such a quantum regime the Coulomb energy U itself is a self-consistent function of the disorder potention $e\langle V_D \rangle$ through the interdependence of the cyclotron orbit radius of the single quasiparticles ($l^2_{CR}=h/2\pi eB$) and the disorder induced electron energy dependent Anderson localization length of the center of mass motion (l_L). Indeed l_L is in turn a self-consistent function of U, B and $e\langle V_D \rangle$. To our knowledge, this self-consistent inter-dependence of the Coulomb interaction and single particle localization effects as a function of increasing B for a given electron density n (i.e. decreasing ν) has not yet been taken into

account in any description of the nature of the states of a 2DEG system. In the absence of such a description, it appears to have become customary to guide one's expectations on the basis of the arguments advanced for the case of zero B field (i.e. the classical Wigner solid, CWS): as a function of ($e<V_D>/U$) the following three regimes are identified based upon expected reasonableness of a zeroth order starting point for the description of the system ground state; (i) ($e<V_D>/U)>>1$ for which single particle localized states is likely a good starting description, (ii) ($e<V_D>/U)<<1$ for which a starting CWS state described in terms of a correlation length is likely a good starting description with the weak disorder inducing pinning of the CWS lattice with respect to the lattice of the host material, and (iii) ($e<V_D>/U$) ~1, an intermediate regime and most difficult to describe but most likely representing a kind of "glassy" ground state.

To have access to the QWS state with present day laboratory capabilities, ultra-low density ($n<5x10^{10}/cm^2$) 2DEG with very low disorder scattering is needed so that $\nu<<1$ can be realized with reasonable B fields in dilution refrigerators providing temperatures down to ~10mK. For this objective alone it is inconsequential whether the electron gas is realized within the conventional Normal heterostructures or the Inverted heterostructures as we undertook and demonstrated through the results summarized in the preceding subsection. It is also immaterial whether the objective was realized through the use of special features in the grown structures, such as short period superlattice buffers, δ-doping, and unusually thick (~1000A) spacer layers or not. However, since realizing inverted structures with ultra low density features was an outstanding challenge of understanding the materials science of growth we took up this challenge as well and, as demonstrated by the results of figures 2 and 3, remain the only group which has successfully overcome the challenge.

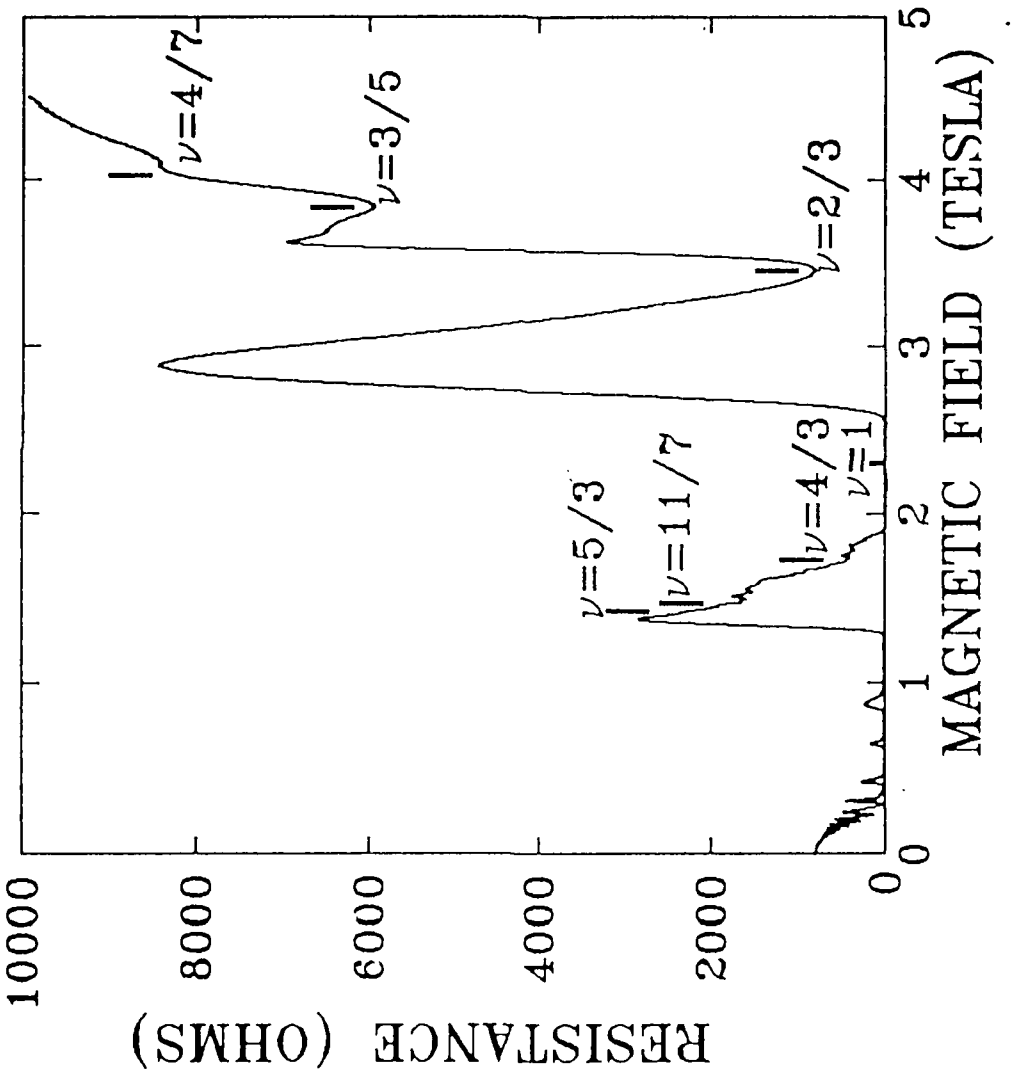
RESISTANCE (OHMS)
10000
8000
6000
4000
2000
0
0
1
2
3
4
5
MAGNETIC FIELD (TESLA)
ν=4/7
ν=3/5
ν=2/3
ν=5/3
ν=11/7
ν=4/3
ν=1

Fig. 5(a)

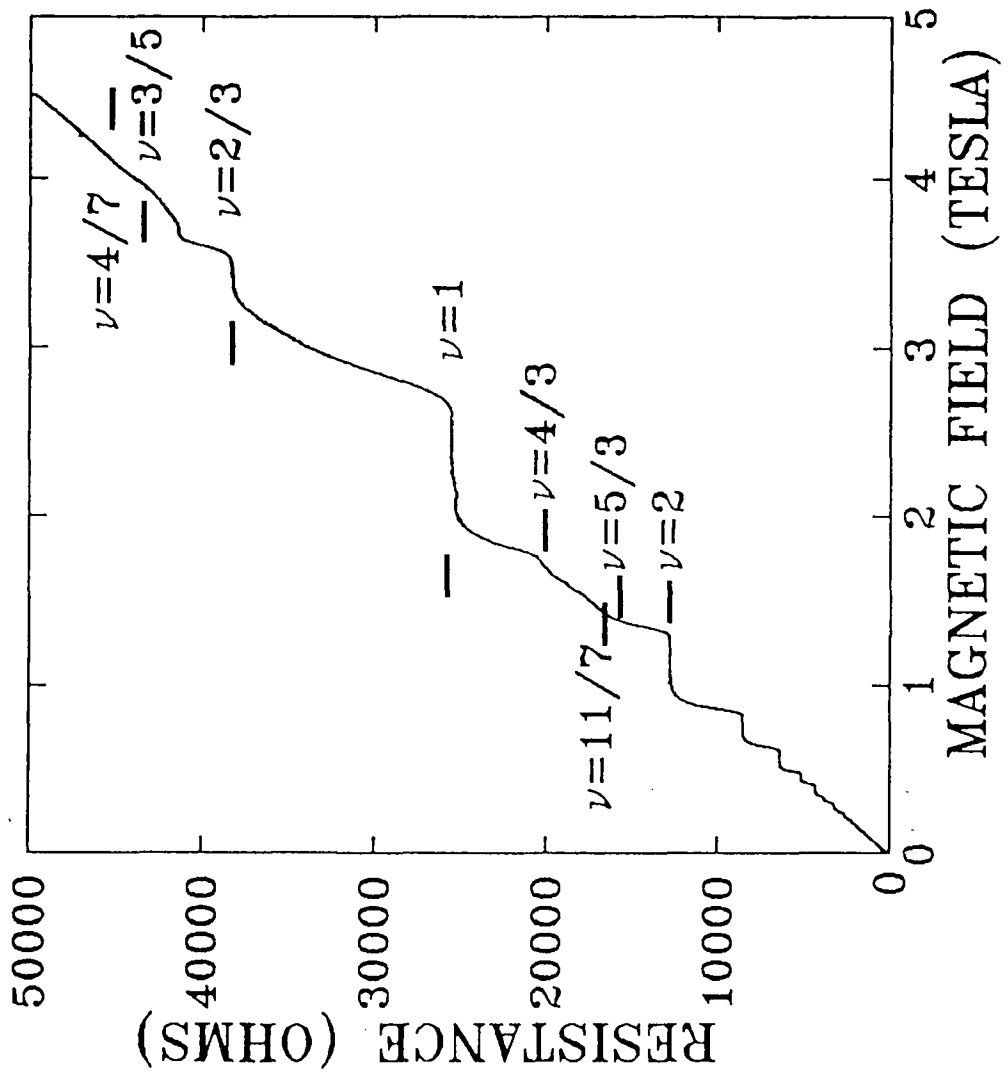
RESISTANCE (OHMS)
50000
40000
30000
20000
10000
0
0
1
2
3
4
5
MAGNETIC FIELD (TESLA)
ν=4/7
ν=3/5
ν=2/3
ν=1
ν=4/3
ν=11/7
ν=5/3
ν=2

Fig. 5(b)

Having achieved ultra-low density 2DEG as early as late '87 we proceeded to examine its magneto-transport behavior but were unfortunately limited by lack of access to appropriate instrumentation: mK regime of temperature and high (B ~15T) magnetic fields. Consequently, we had to be content with ρ_{xx} and ρ_{xy} measurements at 4.2K and B up to ~7T. However, starting late '88 we were successful in establishing collaborative efforts with Prof. H.M. Bozler (of USC) who has dilution refrigerators providing temperatures down to 10mK even though the magnet could go only up to 1.4T. Measurements were carried out on VanderPauw and Hall bar geometry samples to at least examine their IQHE behavior while a parallel effort was mounted to construct a magnet consistent with the space limitations of the sample region of the dilution refrigerator and providing the maximum B-field possible. This turned out to be just under 5T. Results of ρ_{xx} and ρ_{xy} measurements at 20mK on the I-HEMT RG890213 (same as used for figs. 2 and 3) at an electron density of $5.2 \times 10^{10}/cm^2$ are shown in figures 5(a) and 5(b), respectively. Apart from the IQHE seen, FQHE is clearly seen at ν=2/3, 3/5 and 4/7 for the first time in an inverted heterojunction - yet another confirmation of the high quality (i.e. low disorder potential) of the sample. **Details are provided in publication no. 19.** These samples are ideally suited for examining the behavior for B fields up to 15T for which $\nu << 1/5$ regime will be reached - the regime where QWS effects are expected to begin to manifest themselves. Attempts to make collaborative arrangements at appropriate places providing access to this regime have been underway since early '89 and we hope that something would materialize soon for it is truly frustrating to have achieved the harder task of realizing the long elusive appropriate samples but not have the facilities to carry out the truly exciting measurements so long sought after by so many.

(I.2) VERTICAL TRANSPORT:

Electron transport across interfaces offers several interesting studies of the tunnelling phenomenon as well as the potential for new types of devices. In particular, resonant tunnelling has attracted considerable interest in the past few years - both in the context of the basic physics underlying the process and the potential for extremely fast devices. Our interest in resonant tunnelling arises from both these context with particular interest in exploring ways of achieving high peak currents ($\geq$ 100 KAmp/cm^2) and peak-to-valley ratio (>5) through growth of appropriate materials. We initiated our studies through growth of GaAs/$Al_xGa_{1-x}As$(100) resonant tunnelling diodes, eventually moving towards the GaAs/(InAs/AlAs) material system.

(I.2.A) GaAs/$Al_xGa_{1-x}As$(100) RTD's:

We have grown and processed several GaAs/$Al_xGa_{1-x}As$ resonant tunnelling diodes. The generic structure (fig. 6a) consists of a 1 μm thick Si-doped (N_D~1E18/cm^3) GaAs buffer grown on top of a n^+ GaAs substrate, 18 monolayer (ML) undoped GaAs spacer, two 18 ML undoped $Al_xGa_{1-x}As$ barriers with a 20 ML undoped GaAs well sandwiched between them, 18 ML undoped GaAs top spacer and a 0.6 μm n^+ Si-doped (N_D~1E18/cm^3) GaAs cap layer. Samples with barrier composition x=0.3, 0.5, 1.0 have been grown for the purpose of studying the effect of different barrier heights, and the effects of direct-to-indirect gap barrier on the peak to valley ratio (PVR) and the peak current density of the negative differential resistance (NDR) feature in I-V characteristics of the device. All of these samples were grown dynamically (i.e. without any growth interruption at heterointerfaces). A sample with x=0.3 was grown with growth interruption at the heterointerfaces to compare with its counterpart.

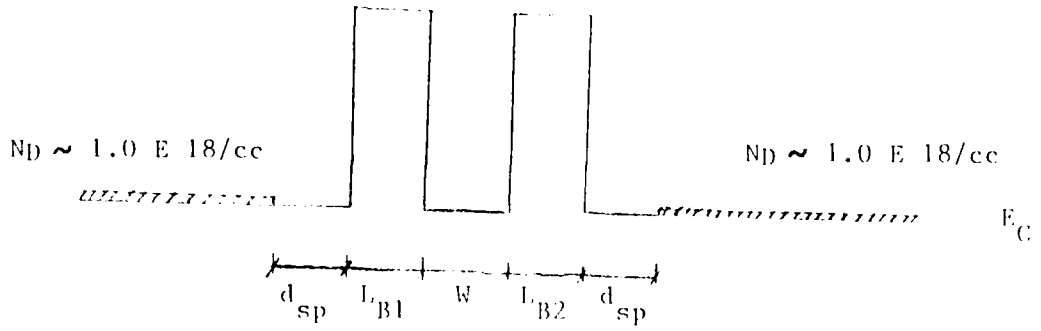

Figure 6a Schematic of Resonant Tunneling Diode conduction band profile. The spacers and well are undoped GaAs while the barriers are undoped $Al_xGa_{1-x}As$.

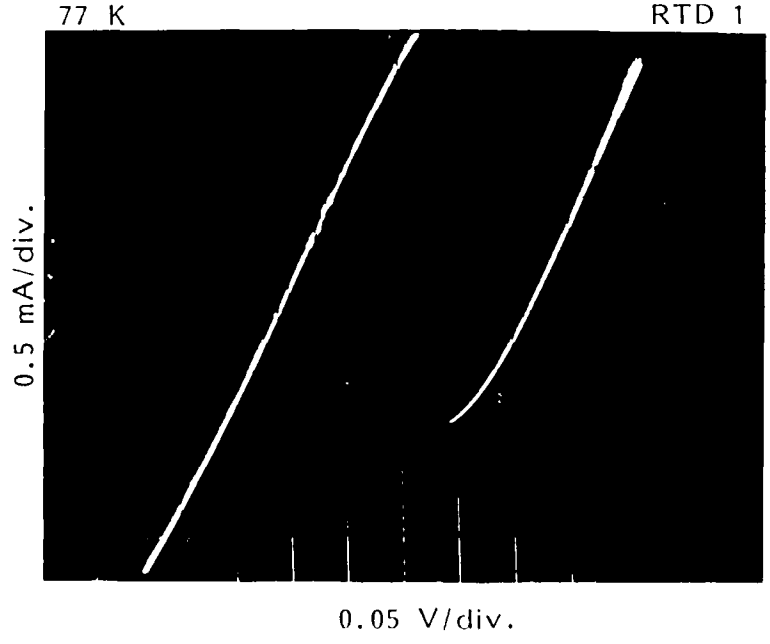

Figure 6b I-V curve of RTD 1 having 30% Al barriers measured at 77 K. The device dimension is 12 x 12 um. This device shows a Peak to Valley Ratio of 3.3 with a peak current density of 3.5 kA/cm^2. Note that origin of I-V curve is shifted to bottom of third quadrant.

All of the above samples were processed into 100 μm x 100 μm and 12 μm x 12 μm square mesas with alloyed AuGe/Ni/Au Ohmic contacts on top and a large area alloyed In contact at the bottom of the chip serving as the bottom contact. Devices processed from all of the samples show NDR at a temperature of 77K as well as 300K. A representative I-V curve is shown in figure 6(b) for x_{Al}=0.3, non-interrupted growth. A PVR of 1.8:1 at 77K with a peak current density of 4.3 KA/cm^2 is seen. This high peak current density for x_{Al}=0.3 is among the best reported in the literature. The I-V curve shows hysteresis due to extrinsic effects such as lead resistances, as well as due to the intrinsic phenomenon of well charging.

(I.2.B) PSEUDOMORPHIC GaAs/$In_xGa_{1-x}As$/AlAs RTD's

Having successfully grown state of the art lattice matched GaAs/$Al_xGa_{1-x}As$ we moved next towards successful realization of the lattice mismatched GaAs/$In_xGa_{1-x}As$/AlAs RTD's. While much of the basic effort on the fundamental aspects of high quality lattice mismatched growth was carried out under other sponsorship, the resulting identification of appropriate growth conditions with increasing In content (i.e. lattice mismatch) were used to produce RTD structures for processing and examination of their I-V characteristics.

A new idea we introduced to enhance the PVR and reduce the valley leakage (non-resonant) current is the use of $In_xGa_{1-x}As$ "spacer" layers between the emitter (base) and first (second) AlAs barrier. This leads to a triple well - double barrier configuration as shown in fig. 7. Samples with and without $In_xGa_{1-x}As$ spacers were grown at a variety of growth conditions. An illustrative set is shown in Table 1. Figs. 8(a) through (d) show comparative I-V characteristics for RTD structures containing $In_{0.1}Ga_{0.9}As$ wells and AlAs barriers. A PVR of 3.2 and peak current of ~10KA/cm^2 is achieved at room temperature - the highest to date

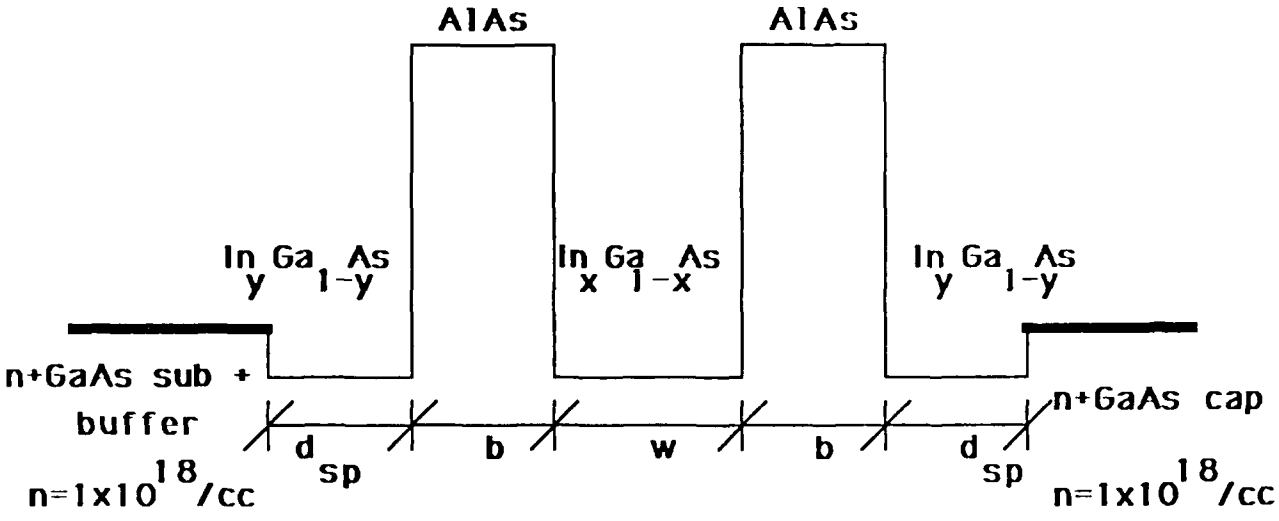
AlAs
AlAs
In y Ga 1-y As
In x Ga 1-x As
In y Ga 1-y As
n+GaAs sub +
buffer
n=1x10 18 /cc
d sp
b
w
b
d sp
n+GaAs cap
n=1x10 18 /cc

Fig. 7

Table 1. Structural parameters of the RTDs studied. The spacer, AlAs barrier, and the $In_{0.1}Ga_{0.9}As$ well layer thicknesses are denoted by d_{sp}, b and w, respectively and given in units of monolayers (1ML=2.83 Å).

Structure #	Spacer material	d_{sp} (ML)	b (ML)	w (ML)
RTD#6	GaAs	18	10	19
RTD#9	GaAs	18	10	25
RTD#10	GaAs	18	10	19
RTD#11	$In_{0.1}Ga_{0.9}As$	18	10	19

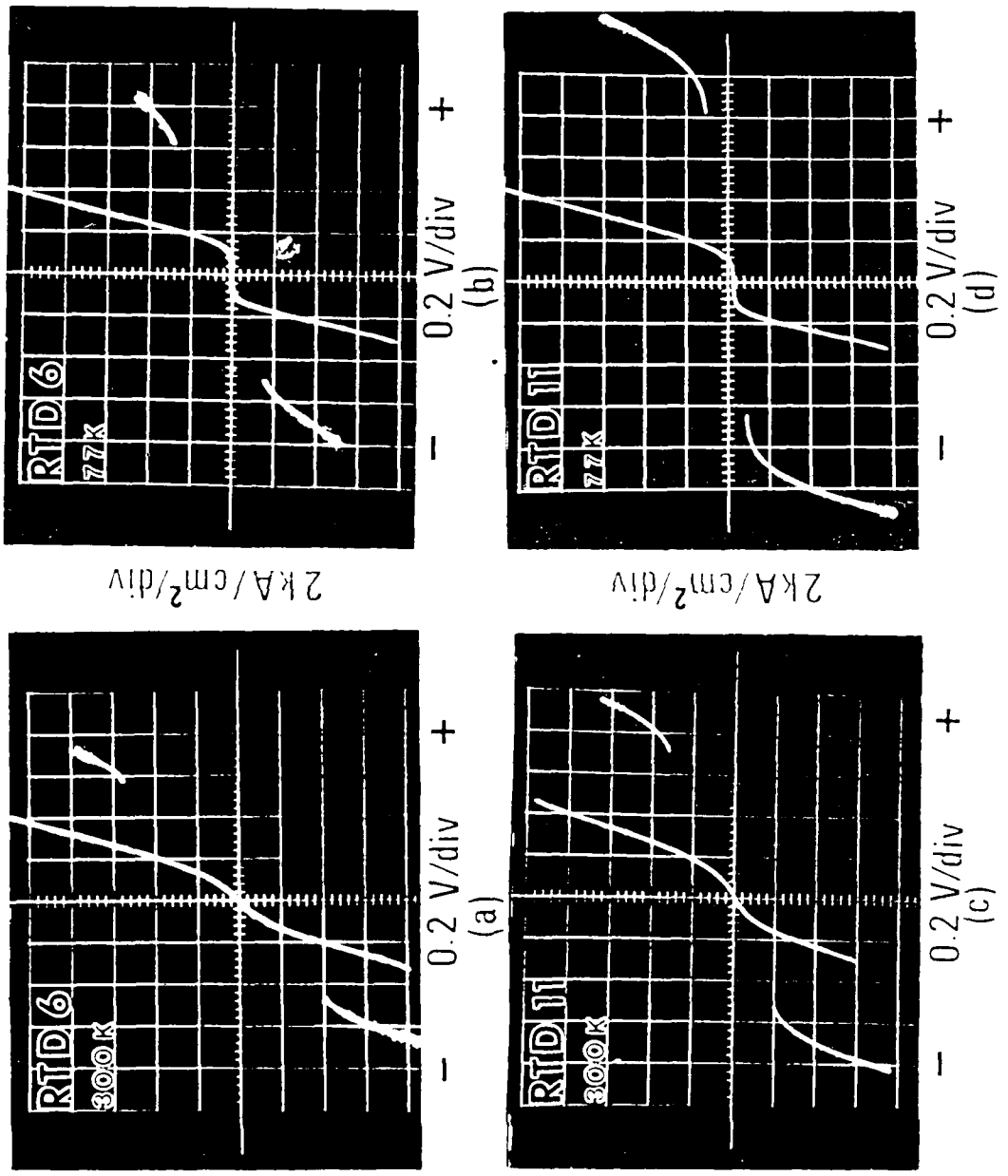
RTD 6
77K
0.2 V/div
(b)
2kA/cm²/div
RTD 11
77K
0.2 V/div
(d)
2kA/cm²/div
RTD 6
300K
0.2 V/div
(a)
RTD 11
300K
0.2 V/div
(c)

Fig. 8

for 10% In and grown directly on GaAs(100) substrates. Furthermore, through calculations of the I-V characteristics we also identified, for the first time, the tunnelling occurs via the Γ-X-Γ-X-Γ band edge path but with the transverse effective mass of the X-point of the AlAs barriers (rather than the longitudinal mass found for the lattice matched GaAs/AlAs RTD structures), a consequence of the presence of strain. **Further details may be found in publication no. 20.**

(I.2.C) RTD's ON PRE-PATTERNED SUBSTRATES:

While increasing In content can improve the PVR and Jp by increasing the well-to-barrier band edge discontinuity, the accompanying increase in strain poses a fundamental challenge to realizing strained structures with low enough defect density. Following our earlier demonstration of strain relief at the free surfaces of growth on measas pre-patterned onto substrates we undertook growth of $In_xGa_{1-x}As$/AlAs RTD's with x up to 0.40 on substrates containing non-patterned regions as well as mesas of dimensions ~ 18 μm x 18 μm. For x up to 0.25 no difference in the RTD characteristics was found between the non-patterned and patterned growth, as seen in fig. 9. The PVR and J_P at room temperature were pushed to 4.5 and 110 KA/cm^2, the highest to date for this system. The lack of difference between the patterned and non-patterned regions is a consequence of the thickness of the $In_xGa_{1-x}As$ layers involved being below the so-called critical thickness for x up to 0.25. However, for x=0.30 while no NDR was found for conventional growth on non-patterned region of the substrate, the patterned region showed NDR. The PVR is considerably degraded giving a value of 1.1. This is a consequence of the growth mode at x > 0.28 changing to a 3D island mode (rather than a layer-by-layer mode) within the designed thickness of the $In_{0.3}Ga_{0.7}As$ spacer and well

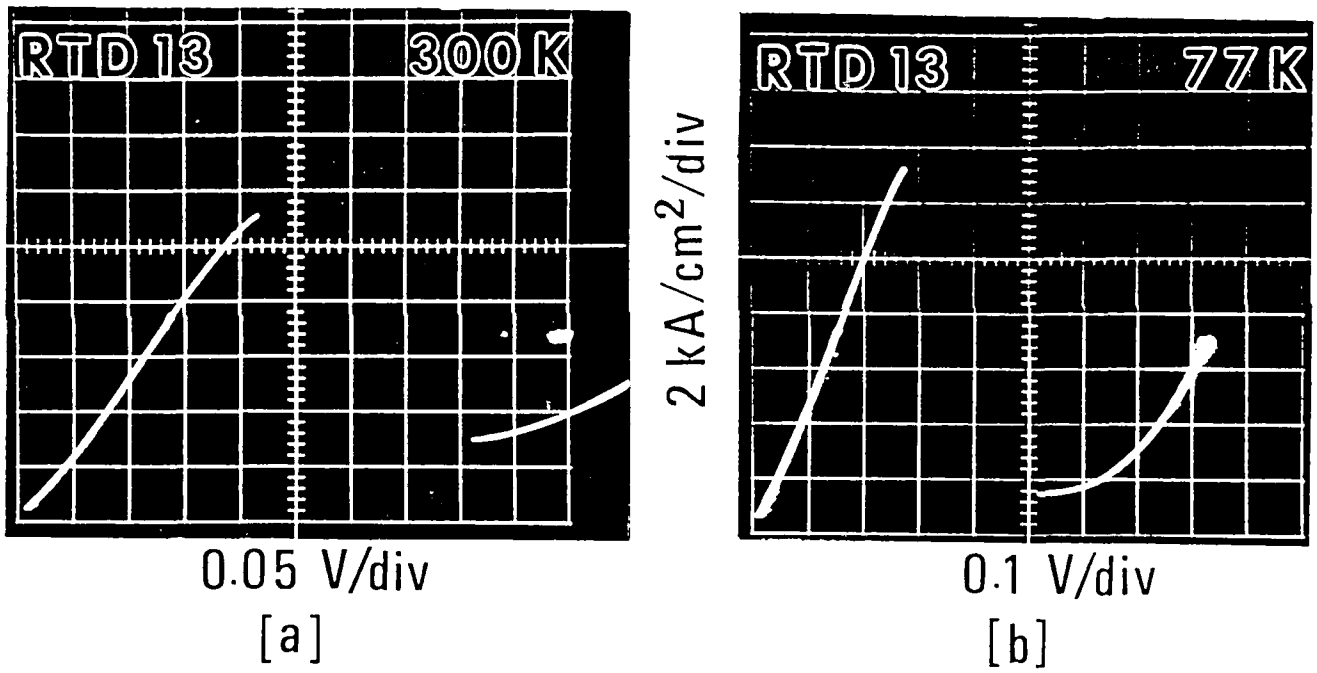

Fig. 9

layers, thus causing presence of structural defects. Further investigations are continuing. Details of the above noted findings **may be found in publication number 21.**

(I.3) OPTICAL PROPERTIES

During the present reporting period, a wide range of experimental and theoretical studies relating to the optical behavior of GaAs/$Al_xGa_{1-x}As$ based quantum well structures were undertaken. The primary experimental techniques employed were,

Near Band Edge Photoluminescence (PL)

Photoluminescence Excitation Spectroscopy (PLE)

Raman Scattering (RS)

Rayleigh Scattering (RLS)

Electro-Reflectance Spectroscopy (ERS)

Photo-Reflectance Spectroscopy (PRS).

In the following we provide a brief description of some of the more important findings of these experimental studies, some of which address basic issues of the optical properties of relevance to quantum wells and others which address the basic nature of the $Al_xGa_{1-x}As$ alloy barrier layer itself - an aspect which influences the nature of the quantum well but had not been carefully and systematically examined prior to our studies.

(I.3.A) COMBINED RAMAN, RAYLEIGH SCATTERING AND PHOTOLUMINESCENCE STUDIES OF $Al_xGa_{1-x}As$ ALLOYS:

Although the $Al_xGa_{1-x}As$ alloy is an integral part of the GaAs/$Al_xGa_{1-x}As$ system, most commonly employed for creation and study of heterojunctions and square quantum wells, its

properties had not been investigated in a systematic way. Indeed our experimental RHEED studies during growth of $Al_xGa_{1-x}As$ alloys and alloy barrier layers, as well as our Monte Carlo computer simulation studies had indicated that the quality of the alloy layer grown and the atomistic structural and chemical nature of the interfaces formed in quantum well structures must depend upon the kinetics of growth. The successful realization of the high mobilities in the I-HEMT structures discussed in section (I.1) was achieved by manipulating the kinetics based upon these realizations. We therefore undertook an optical investigation as an independent means of examining the correlation between the RHEED and the growth kinetics in an effort to further strengthen the value of RHEED in arriving at optimized growth conditions for realization of high quality alloy layers and quantum well structures.

Systematic Raman scattering and Rayleigh scattering studies of thick $Al_{0.3}Ga_{0.7}As$ alloy layers grown under RHEED indicated optimized and non-optimized conditions were thus undertaken. The combination makes a powerful tool since while Raman scattering is sensitive to alloy disorder activated breakdown of selection rules, the Rayleigh scattering is sensitive to fluctuations in mass density that accompany defects and clustering effects. The studies clearly showed a significantly lower Rayleigh scattering in $Al_{0.3}Ga_{0.7}As$ alloys grown under RHEED optimized growth conditions as compared to samples grown under conditions indicated by the RHEED intensity dynamics to be non-optimal. Consistent with this, the Raman scattering showed significantly lower intensity of disorder activated peaks and the absence of any bulk GaAs-like peak in samples grown under RHEED optimized conditions. These studies thus constitute a direct optical determination of the power of RHEED in identifying optimized growth conditions.

The above noted approach was extended to examination of the quality of $Al_xGa_{1-x}As$ alloys as a function of the Al concentration (x). Note that the main point here is that the differences in the Ga and Al growth kinetics imply that the optimized growth conditions for alloys with differing x values are different. These studies were further supplemented by PL studies, thus gaining complimentary information on various length scales; atomic for Raman, of the order of the exciton size for PL, and long ranged for Raleigh scattering. At high Al concentrations ($x \simeq 0.8$) we showed the occurrence of atomic scale (~10A) GaAs-like and AlAs-like regions in the sample. In addition, AlAs-like TO mode was observed in the forbidden backscattering geometry and, unlike previous suggestions of alloy disorder effect, was attributed to twinning effects in the sample arising from strain effects and dependent upon the growth kinetics. The phonon-assisted excitonic recombination in the indirect band gap region ($x>0.42$) was, unlike earlier explanations, shown to involve phonon around the X and L points as well, even though the dominant contribution arises from phonons around the X-point.

Another finding, of considerable pragmatic value and which comments on the common usage of PL and Raman scattering as a means of post-growth determination of alloy concentration, is that the prevalent expressions employed routinely for such interpretation are not reliable to an accuracy better than $\pm 5\%$. In many cases, the discrepancy found within a given technique (PL or Raman) employing commonly used expressions (empirical or theoretical) for two different peaks is as large as 20%. A critical need for much more reliable theoretical expressions as well as empirical relations thus exists.

The details of these studies may be found in **publication nos. 8, 12 and 15.**

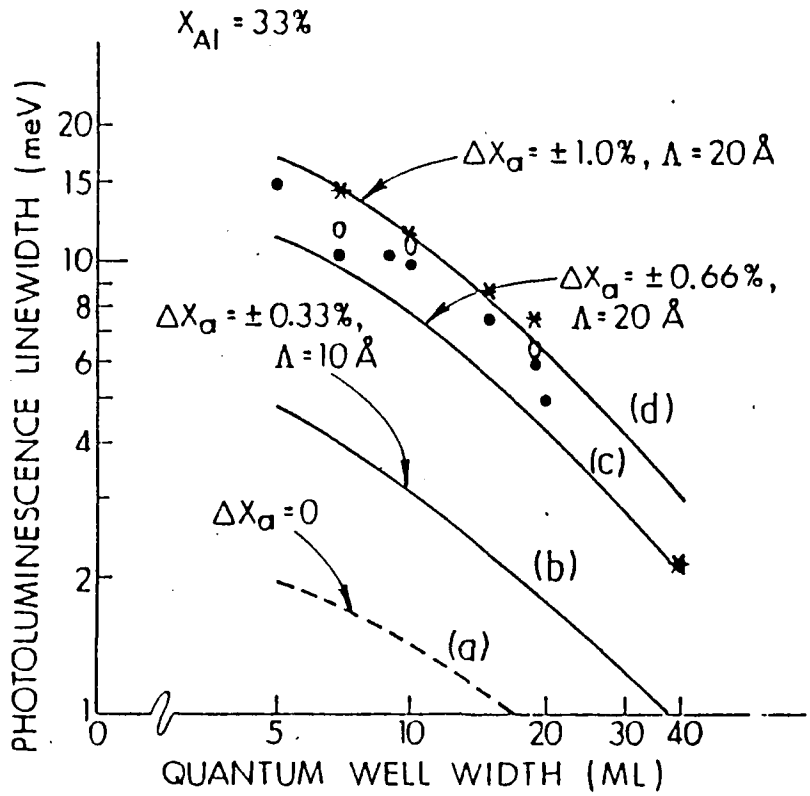

The measured dependence of the PL linewidth on the quantum-well width d_w. Solid circles and asterisks indicate data taken at 5 K and 40 K, respectively. The open circles are linewidths determined in PL excitation spectra taken at 5 K. The dashed line corresponds to the theory, retaining only the microscopic alloy-disorder contribution, while the solid lines correspond to the results obtained with inclusion of varying degrees of composition fluctuation of amplitude ΔX_a and correlation length Λ.

FIGURE 10

(I.3.B) THE PL LINE WIDTH DEPENDENCE ON WELL WIDTH:

Through a systematic examination of the low temperature (4K to 40K) PL and PLE excitonic line widths as a function of well width in single square quantum wells of $GaAs/Al_{0.3}Ga_{0.7}As$ grown under identical and RHEED optimized growth conditions, we had found (see fig. 10) that $\Gamma_{PL} \alpha d_w^{-1}$ rather than $\Gamma_{PL} \alpha d_w^{-3}$ as predicted by the prevalent notion that it is the well width fluctuation which is the line width determining factor. This popular notion and model having been ruled out by our experimental findings, we were naturally faced with the task of finding out what gave rise to the observed $\Gamma_{PL} \alpha d_w^{-1}$ behavior. (We note the same is true of Γ_{PLE} and for both Γ_{PL} and Γ_{PLE} the same was found to hold up to temperatures as high as 40K).

Based upon our computer simulations of MBE growth of GaAs/ $Al_xGa_{1-x}As$ quantum wells (undertaken under ONR sponsorship) we had already identified the presence of in-plane Al composition fluctuations (i.e. along the interfaces) arising from the differences in the Al and Ga migration and reaction kinetics. Such fluctuations from the intended global composition were found to occur on length scales of 20 to 100A, depending upon the growth kinetics operative under the chosen growth conditions. Thus it was clear to us that the exciton size in the quantum wells being of order 100A (radius), the recombination life time must be influenced by the presence of such local Al concentration fluctuations i.e. fluctuations in the band-edge discontinuity (the depth of the confining potential). Thus under the present ARO Grant we undertook development of a theory of the PL linewidth due to exciton scattering by (a) the band-edge discontinuity fluctuations, and (b) alloy disorder experienced by the exciton due to its wave function penetrating into the alloy barrier layers. The local Al concentration (on the scale of the exciton size) fluctuation correlation function was modelled as a Gaussian.

The calculated line width as a function of well width showed the observed nearly d_w^{-1} dependence, in conformity with the experimental findings. It is perhaps worth noting that, subsequently, Ourzmad et.al.[1] through transmission electron microscope lattice imaging and image simulation studies determined the existence of such Al concentration fluctuations on the length scales of 20-50A, in conformity with our computer simulation findings, as well as substantiating our physical model for the observed $\Gamma_{PL} \sim d_w^{-1}$ behavior.

This work is to be found in **publication no. 1** of the list of publications given in section (II).

(I.3.C) DOUBLE-RESONANCE RAMAN AND OPTICAL PHONON - ELECTRON RESONANT MIXING:

Nearly a decade ago, we predicted[2] a resonant mixing between the two quasi two dimensionally confined electronic states when their separation becomes comparable to an optical phonon energy. Early experimental efforts to observe this phenomena were based on making the cyclotron resonance frequency in a two dimensional electron gas comparable to the optical phonon energy. While some indication of the existence of the phenomena was found in dc measurements (the so-called magnetophonon effect) in GaAs/$Al_{0.3}Ga_{0.7}$As HJ's and in ac measurements in the InAs/GaSb HJ's, the results could not provide as clear information as could be obtained - a consequence of the lack of high enough magnetic fields and electron screening effects. Consequently, we devised the appropriate GaAs/$Al_{0.3}Ga_{0.7}$As SQW structure consisting of 8 or 9 ML wide GaAs well, undoped, for which the light hole (lh) and heavy hole (hh) separation is close to the GaAs bulk LO phonon frequency of ~36 meV. Then, under the resonant excitation condition of $h\nu_{inc}$ = (lh-e^-), the outgoing single phonon Raman

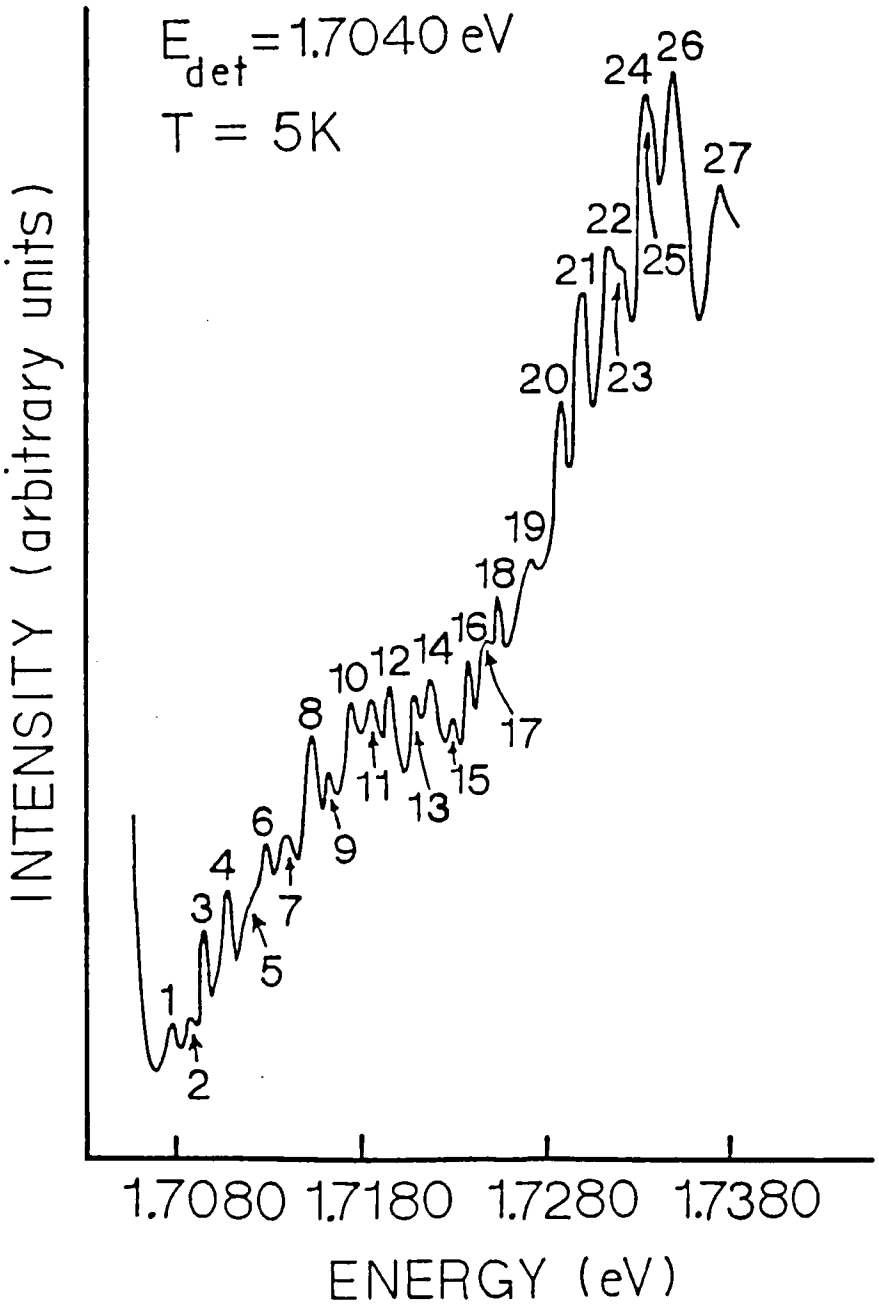
E det = 1.7040 eV
T = 5K
INTENSITY (arbitrary units)
1
2
3
4
5
6
7
8
9
10
11
12
13
14
15
16
17
18
19
20
21
22
23
24
25
26
27
1.7080
1.7180
1.7280
1.7380
ENERGY (eV)

Fig. 11

photon satisfies $h\nu_{out}=(hh\text{-}e^-)$, thus creating a DOUBLE RESONANCE condition, enhancing Raman cross section dramatically. Consequently, in the secondary emission spectra we observed the double Resonance Raman Scattering (DRRS) lines corresponding to three optical phonons, along with the usual photo luminescence. In the PL excitation spectra (a sort of analog of absorption), a remarkable 27 peaks were observed riding over the step-like quasi 2D density of states (see fig. 11). These peaks were shown to correspond to a radical modification of the 2D density of states due to resonant mixing of 16 different optical phonons of the SQW structure with the light and heavy hole states. These 16 phonons were shown to belong to the categories of confined in the well, confined in the barrier, interface, and unconfined phonon states of a square quantum well structure. This is, and remains, the only simultaneous observation of all possible phonon states of a SQW structure, apart from providing a clear and unambiguous confirmation of our theoretical predictions. Details may be found in **publication nos. 6 and 7.**

(I.3.D) POLARIZATION BEHAVIOR OF EXCITONIC RECOMBINATION IN SQW'S:

Although the polarization behavior of bulk semiconductors (such as GaAs) has been shown to provide useful information on the momentum and energy relaxation of the photoexcited carriers, studies of the polarization behavior of excitonic recombination in confined structures had not been undertaken prior to our studies. We examined this behavior for both, ordinary SQW structures and the double resonance SQW structure discussed in the preceding. The ordinary SQW structures exhibited little or no linear polarization. The double resonance SQW's, on the other hand, showed a strong linear polarization dependence on the incident photon energy. They also showed a reduction in the PL linewidth. These effects

were attributable to the strong modification of the confined heavy hole level due to the resonant mixing with the light hole level brought about by the optical phonon. Details are to be found in **publication no. 13.**

(I.3.E) THE QUANTUM CONFINED STARK EFFECT:

It has been shown that the application of an electric field across a square quantum well causes the excitonic absorption to shift to lower energy and a broadening of the absorption line width. This effect, dubbed the quantum confined Stark effect (QCSE) is a consequence of the shifting of the confined electron and hole wave functions away from each other due to the tilting of the quantum well potential under applied field. The QCSE is of some significance for it can be exploited for the creation of light amplitude modulation based spatial light modulators (SLM). It has been employed in a p-i-n configuration integrating the detection and modulation functions to create the self-electrooptic effect device (SEED)[3]. A basic limitation on the modulation depth achievable in devices based on the QCSE arises from the absorption broadening. Two basic mechanisms contribute to this broadening; (i) the broadening due to various departures from ideal quantum, well behavior present at zero and non-zero fields and (ii) broadening arising from tunnelling if the applied field becomes large enough. The conventional model for the former had been the usual well width fluctuation mechanism. However, as discussed in section (I.3.B), our PL experiments showed that the zero field line width is dominated by fluctuations in the band edge discontinuity and alloy disorder scattering. Consequently, we undertook a theoretical analysis of the influence of an electric field on the PL line width arising from these two dominant sources.

The PL line width was calculated as a function of applied field (0 to 100 KV/cm) for varying well widths and barrier layer global alloy composition for the GaAs/$Al_xGa_{1-x}As$ SQW system. We showed that for a given well width (particularly >100A), the increase in line width with applied field is very sensitive to the degree of Al concentration fluctuations in the interface plane. The higher the amplitude of such fluctuation correlation function, the more rapid the increase in the line width and hence, the less the absorption modulation. Thus once again, the control on the kinetics of growth through usage of optimized growth conditions is seen to be a key issue. Further details are to be found in **publication no. 3.**

(I.3.F) COUPLED-DOUBLE QUANTUM WELLS:

A coupled double quantum well (CDQW), shown schematically in fig. 12(a), gives rise to symmetric (S) and antisymmetric (AS) combinations of the individual isolated well states, the energy splitting being controlled by the width and height of the barrier layer. The electric dipole selection rules for absorption permit only S-S and AS-AS transitions under flat band conditions. Upon the application of an electric field, the tilting of the CDQW potential makes possible mixed transitions which gain oscillator strength at the expense of the S-S and AS-AS transitions. This physical process offers an interesting alternative to the QCSE for achieving amplitude and/or phase modulation. Thus to gain a feel for the magnitude of changes in n and K we undertook calculations based upon a phenomenological approach which modelled the excitonic transitions as Lorentzian oscillators, the 2D density of states effect as a broadened step function, and the contribution of the unconfined states as a rising background. This lattermost contribution is essential to achieving a correct description of the underlying physics since even the behavior in the limited energy range of the confined states

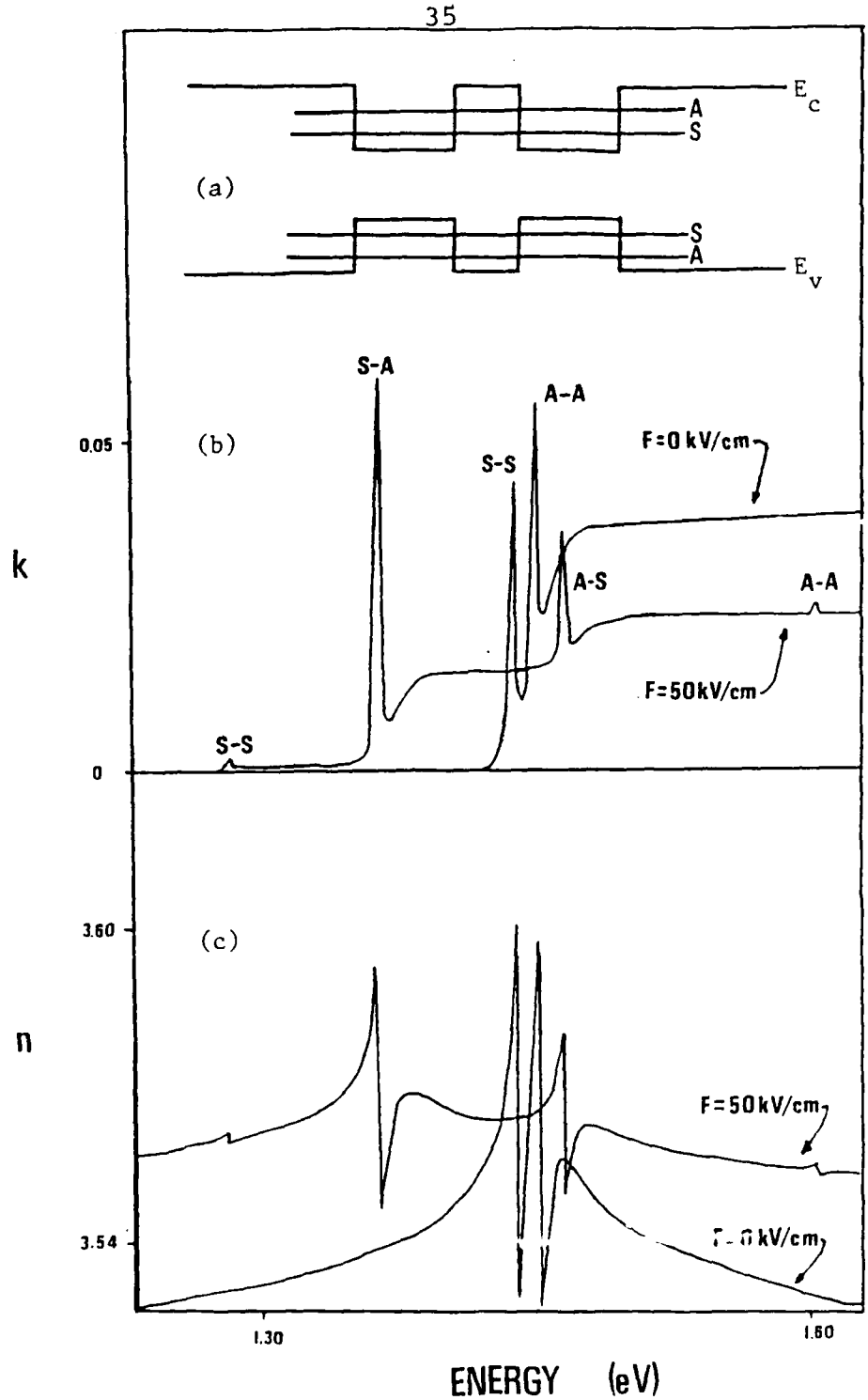

Fig. 12 (a) Shows schematic band diagram of CDQW under flat band conditions with the symmetric (S) and antisymmetric (A) confined electron and hole energy levels.
(b) Shows absorption coefficient k as a function of transition energy for 0 and 50 kV/cm total field based on phenomenological model.
(c) Shows index of refraction n as a function of transition energy for 0 and 50 kV/cm total field based on a phenomenological model.

is dramatically influenced by all other states - a consequence of the fact that all states are eigenfunctions of the same Hamiltonian so that n and K in the confined state energy regime are significantly controlled, through the Kramers-Kronig relation, by their behavior at energies far away. An example of the calculated behavior for 40 ML GaAs wells coupled through a 5 ML wide $Al_{0.3}Ga_{0.7}As$ barrier layer is shown in fig. 12. One not only notices the build-up of the oscillator strengths in the transitions forbidden under flat band conditions, but also that at sufficiently large fields the AS heavy hole to S electron transition can be pulled below the band gap of the GaAs substrate. Consequently, a large change in the absorption, going from the subband gap residual absorption ($\alpha<10cm^{-1}$) to the high absorption ($\alpha\sim10^{4}cm^{-1}$) at the mixed transition appears possible. Similarly, in other energy regime a significant change in n without a large change in K appears possible - a feature highly desirable for phase modulation based spatial light modulators.

Given the potential of CDQW, we undertook a systematic experimental study. Starting early '87, a large number of CDQW of varying well and barrier width were grown under RHEED optimized growth conditions on our Φ-400 MBE machine and their PL and PL excitation spectra examined as a function of applied bias. Two major experimental push-ups were necessary to undertake such a study. **First**, considerable effort went into optimizing the deposition conditions and thickness of the transparent metal gate - indium-tin oxide (ITO)- along with the thickness of the $Al_{0.3}Ga_{0.7}As$ barrier layer immediately below so as to prevent damage to the CDQW structure during ITO deposition and to minimize ambiguities due to ITO induced strain effects in the CDQW. This part of the work was undertaken in collaboration with Prof. A.R. Tanguay, Jr. and his students with whom we evolved a collaborative effort on SLM's under the context of the URI on "Integration of Optical

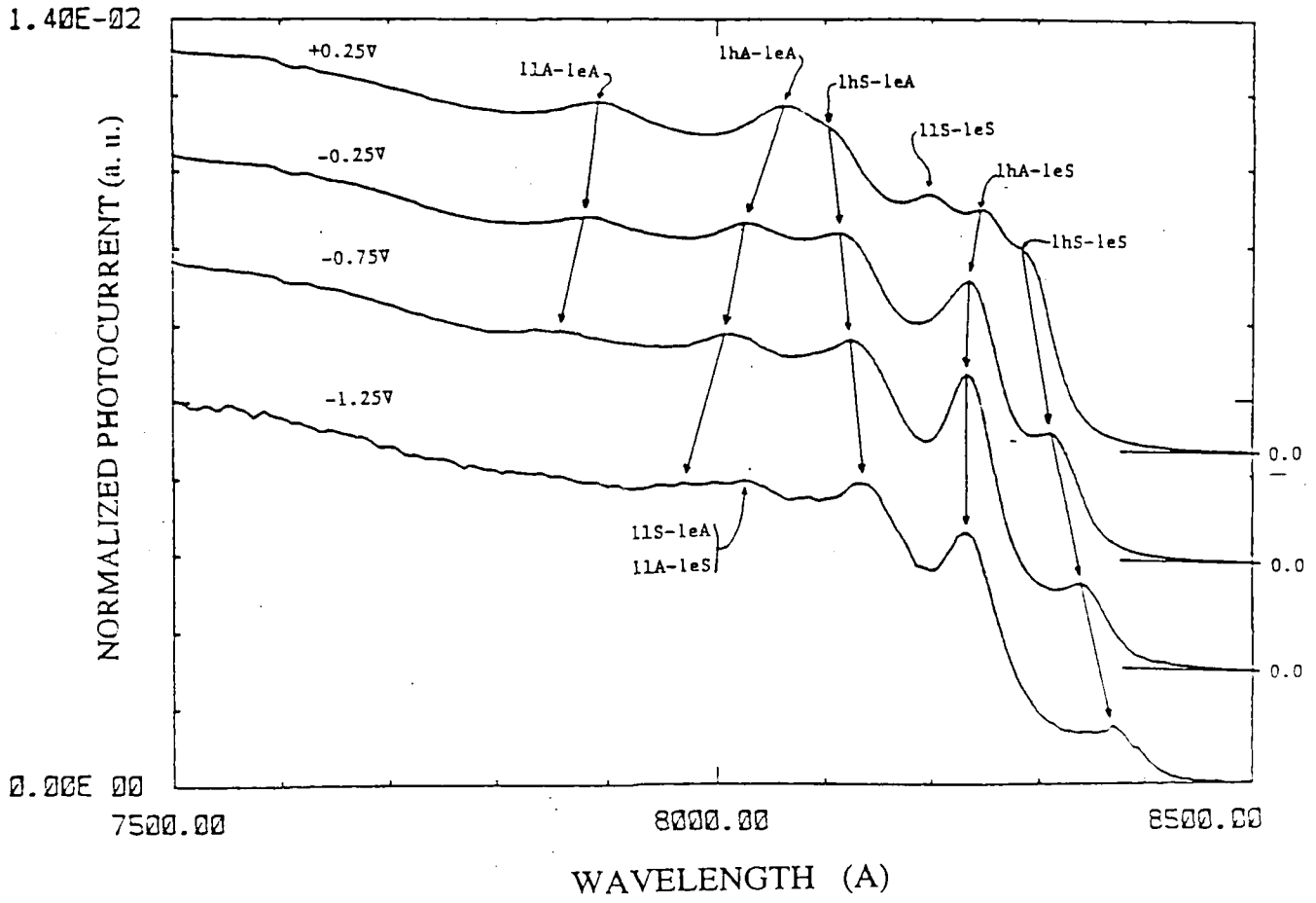

Fig. 13 Photocurrent spectra on a 20-5-20 monolayer CDQW with 20 pairs at room temperature for-0.25V (forward bias), and -0.25V, -0.75V, -1.25V (reverse bias). The total thickness of the CDQW region is 5208 A. The nomenclature of the assigned peaks is as in the text. The zero level of each spectrum has been offset.

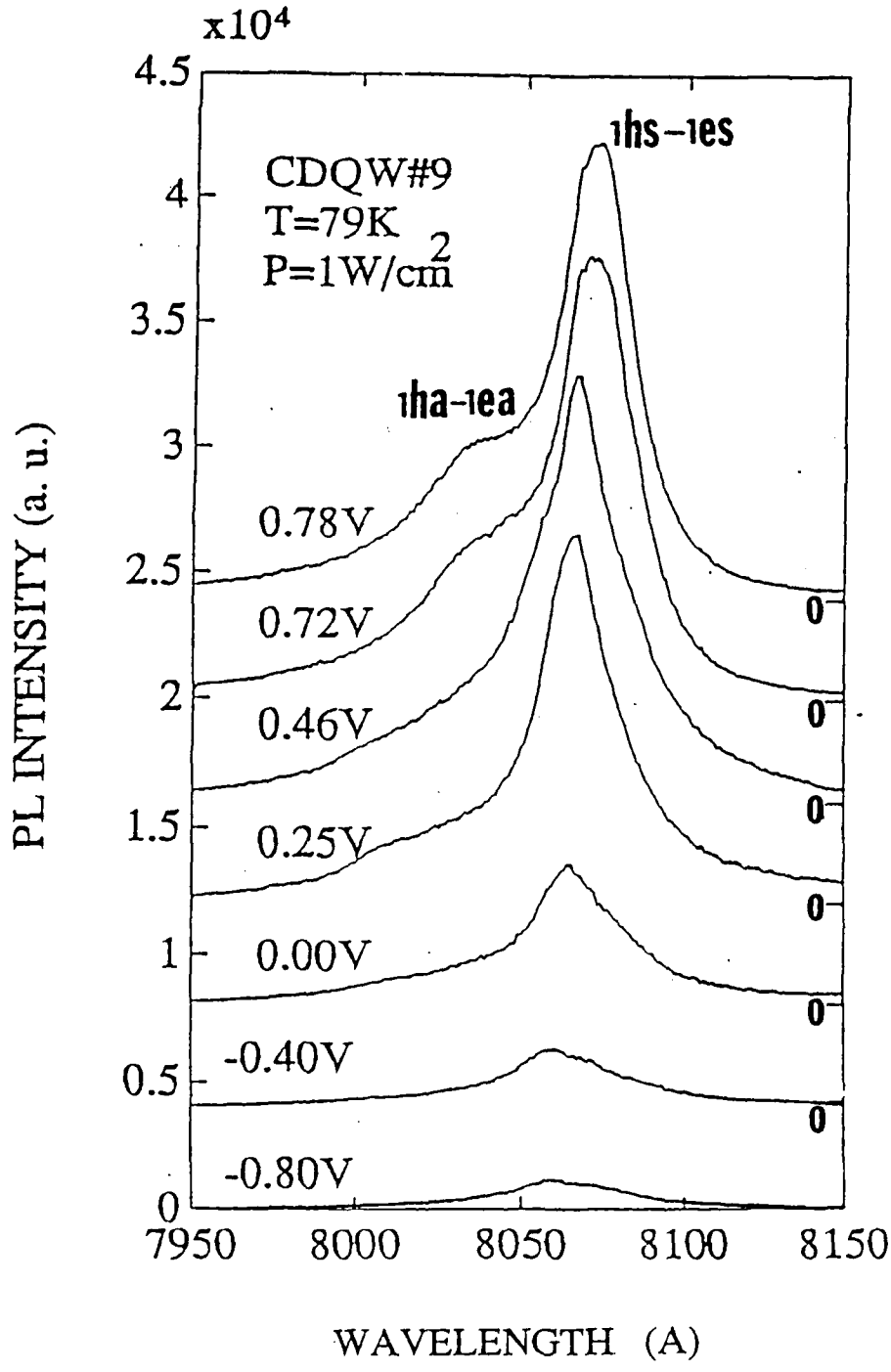

Fig. 14 Photoluminescence spectra on a 40-5-40 monolayer CDQW with 20 pairs at 79 K for 0.78V, 0.72V, 0.46V, 0.25V (forward bias), 0.0V, and -.4V, -.8V (reverse bias). The total thickness of the CDQW region is 7739 A. The zero level of each spectrum has been offset.

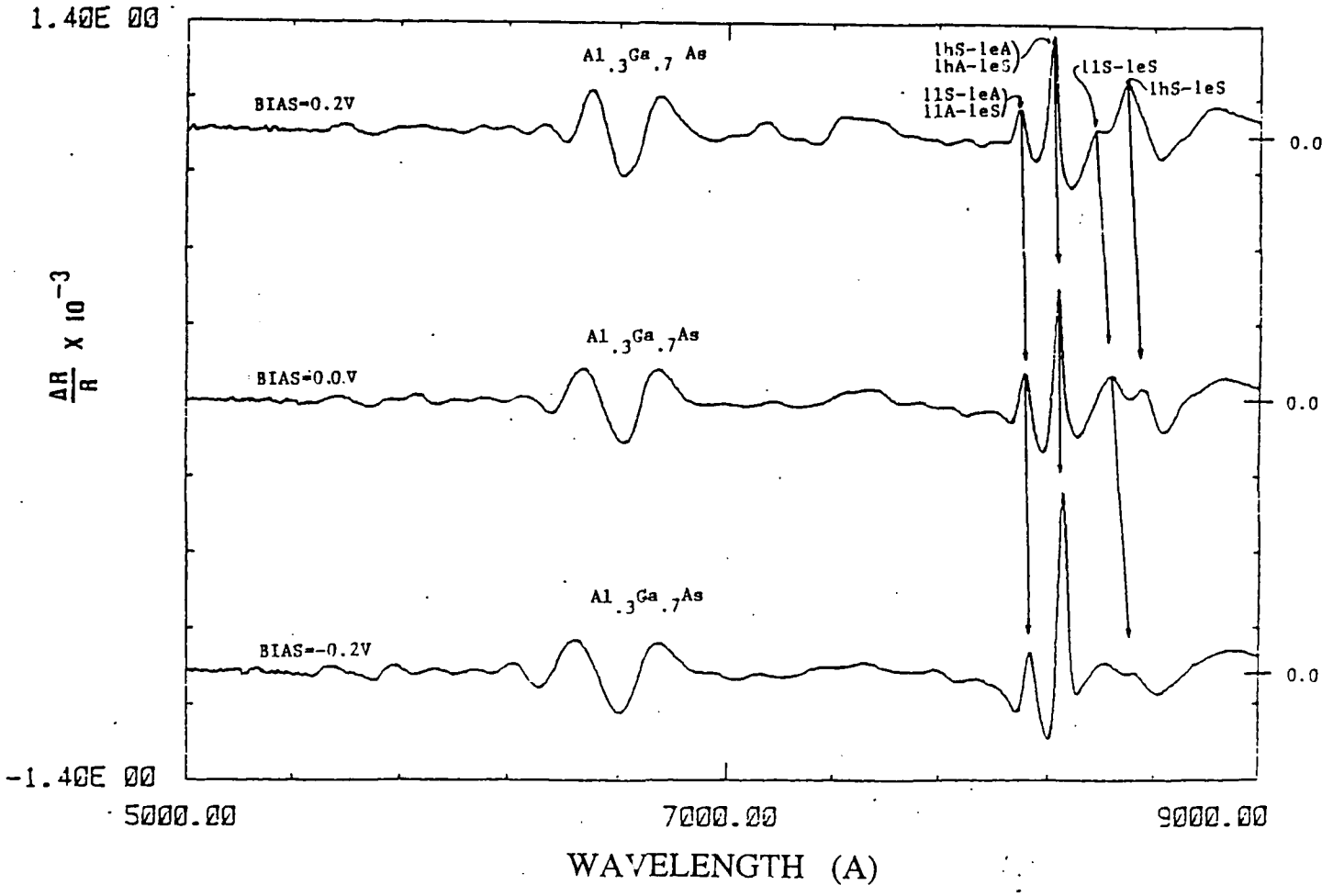

Fig. 15 Electroreflectance spectra on a 20-5-20 monolayer CDQW single pair at room temperature for 0.2V (forward bias), 0.0V, and -0.2V (reverse bias). The total thickness of the CDQW region is 1153 A. The zero level of each spectrum has been offset.

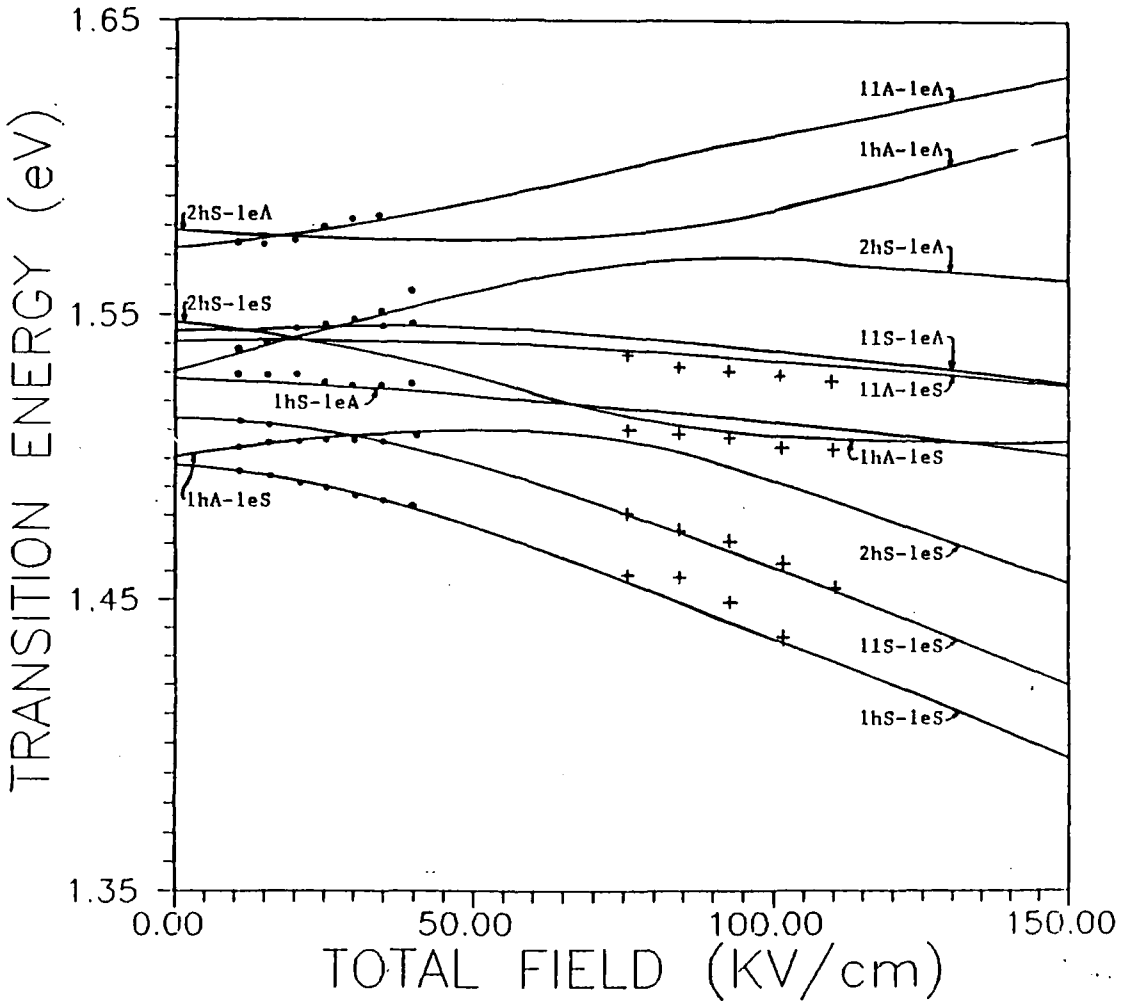

Fig. 16 Calculated (solid line) and measured photocurrent (•) and electroreflectance (+) transition energies as a function of total field for a 20-5-20 monolayer CDQW is shown. The nomenclature of the assigned peaks is in the text.

Computing" at USC. The **second major push-up** starting summer 1987 was in the area of setting up room temperature techniques such as **electro-reflectance** (ER) and **photo-reflectance** (PR). For the GaAs/AlGaAs based systems absorption measurements require etching of the backside substrate with a very high degree of control and uniformity, while at the same time being careful about mechanical strain effects that may arise in a "free-standing" very thin film. Since absorption measurements are eventually the most direct and desirable measurements, a **third effort** begun in parallel was setting-up, at minimal cost, a home-built substrate chemical etching system in which the etching can be monitored via appropriate wavelength light transmission in real time. Setting up the ER and PR measurement systems also required resources not available under the present Grant. Nevertheless, by fall of '87 we established these facilities with some borrowed equipment, tested the measurement system against well known spectra for bulk GaAs and $Al_{0.3}Ga_{0.7}As$, optimized the system for signal to noise ratio and were finally ready by summer '88.

During '88 we undertook extensive studies of the CDQW structures employing PL, PLE, ER, PR, and photo-current (PC) spectroscopies. Some illustrative results are shown in fig. 13 (PC), fig. 14 (PL), fig. 15 (ER) and fig. 16 (comparison with theory). One clearly sees the influence of the applied field. A slight ambiguity that remains in such measurements relates to pin-pointing the exact condition under which the system is in flat-band condition - a consequence of the built-in field in grown structures due to the background doping and defects in the material. The cross checks provided by the simultaneous use of different techniques helps in this process.

(I.3.G) FAR INFRA-RED CYCLOTRON RESONANCE:

In collaboration with Prof. J. Leotin of Institut National des Sciences Appliquees (INSA), Toulouse (France) we undertook far infrared cyclotron resonance measurements on the 2D electron gas in the inverted side doped GaAs/AlGaAs heterojunctions and square quantum wells examined for their transport and magnetotransport behavior as described in section (I.1). The main objective was to obtain informaton on the nature of the inverted interface via its scattering influence on the cyclotron resonance line position and shape and to contrast it with the information extracted from the dc measurements. Indeed, some of the samples included in this study were consciously chosen to be of low mobility to provide a range of inverted interface characteristics. The cyclotron resonance behavior of the high quality inverted structures was found to be essentially the same as found for reference normal heterostructure samples. On the low mobility inverted heterostructures however a very interesting new behavior was revealed in the cyclotron resonance. This is shown in the illustrative example of fig. 17. Note the presence of TWO cyclotron resonance dips in the transmission spectra as a function of the magnetic field (B) at an electron density of ~ $5x10^{11}/cm^2$. Only the usual single dip is present at the lower electron density (fig.17). Identifying the resonance position with the incident photon energy through the usual expression $\omega_c=(eB/m^*c) = E_{inc}$ we obtain two effective masses. The behavior as a function of electron density (magnetic field) obtained for incident wavelengths of 96.5 μm and 119 μm is summarized in fig. 18(a). The interesting issue, of course, is what is the underlying cause of this unusual behavior.

Through experimental considerations we can rule out any contribution due to unintentional tilting of the sample with respect to the magnetic field since this uncertainty is <2°, too small to give rise to a parallel component of the magnetic field big enough to account

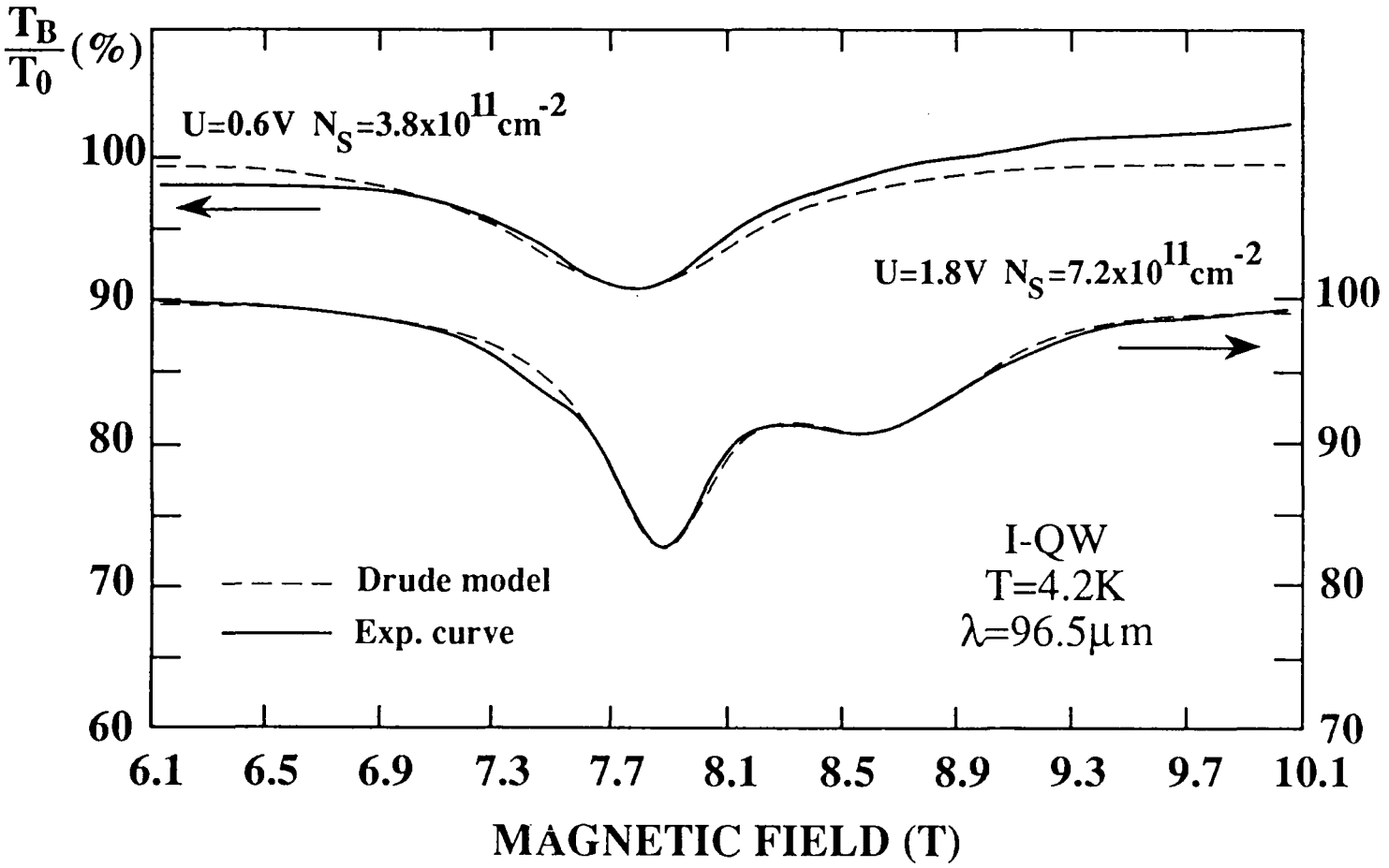
$\frac{T_B}{T_0}$(%)
U=0.6V N_S=3.8x10^{11}cm^{-2}
U=1.8V N_S=7.2x10^{11}cm^{-2}
Drude model
Exp. curve
I-QW
T=4.2K
λ=96.5μm
100
90
80
70
60
6.1
6.5
6.9
7.3
7.7
8.1
8.5
8.9
9.3
9.7
10.1
MAGNETIC FIELD (T)

Fig. 17

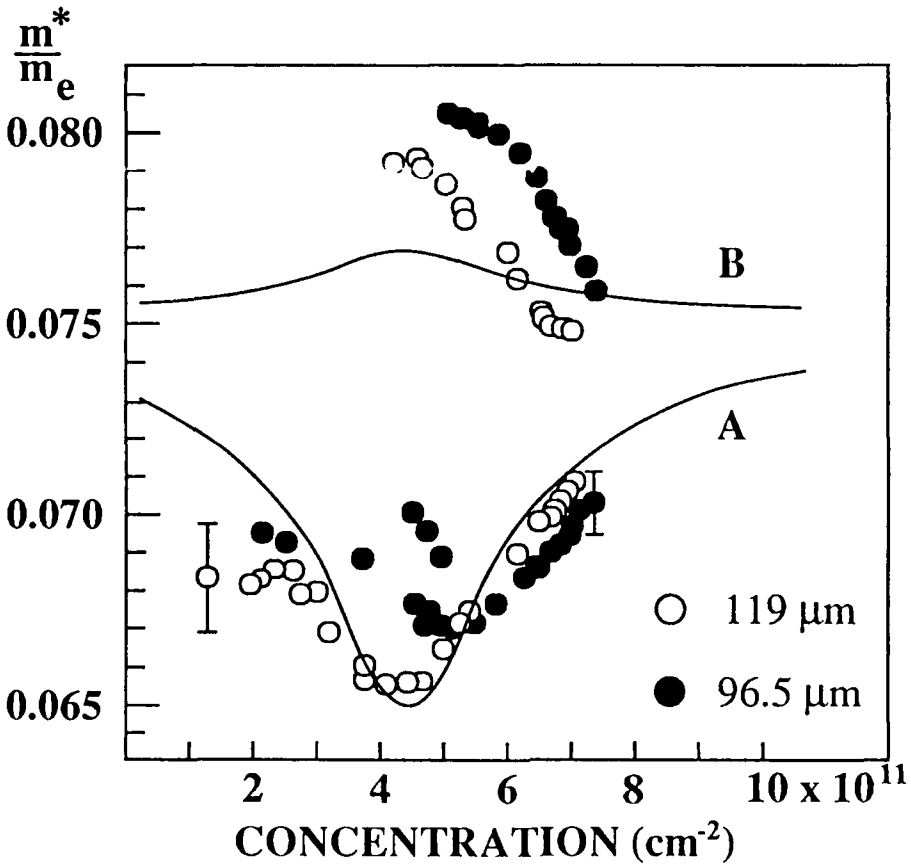
m*/m_e
0.080
0.075
0.070
0.065
B
A
119 μm
96.5 μm
2
4
6
8
10 x 10^11
CONCENTRATION (cm^-2)

Fig. 18

for the observed splitting. Cyclotron resonance splitting observed in normal heterojunctions under conditions of intersubband separation coinciding with an appropriate integer multiple of Y_c can also be ruled out in our case since the situation is far from such a resonance mixing. Our proposed explanation, however, does invoke such a mixing but arising from an inhomogeneous distribution of electric fields in the inverted interface plane. Such a field we propose arises from trapped interface impurities. A model calculation accounting for cyclotron resonance - intersubband mixing arising from such lateral electric fields was undertaken within the perturbation theory framework and including the first three Landau levels of the electric ground state and the first excited state. Fig. 18(b) shows the calculated behavior (solid lines) and the present data (solid circles) along with data (open circles) taken from another study at essentially the same electron density ($4x10^{11}/cm^2$). Details may be found in **publication no.22.**

(I.3.H) LASER ASSISTED AND NON-ASSISTED MBE GROWN GaAs on Si(100):

The system GaAs on Si is of interest for its significance to integration of optoelectronic devices with Si devices and circuitry. The fundamental materials growth and Physics issues that are impeding the progress, however, arise from the lattice mismatch (4% compressive), thermal expansion mismatch, and bonding aspects of a heteropolar material on homopolar substrate. We undertook to examine the optical properties (and structural properties under separate sponsorship by ONR) of THIN (<0.3 μm) GaAs films grown on Si(100) substrates, offcut 4° towards [110], via **MBE UNDER EXCIMER LASER IRRADIATION** to influence the growth kinetics. The growth was carried out under ONR sponsorship. The KrF 248 nm line was used and the irradiation angle and beam (unfocussed) diameter are such that on the 2" Si wafer only a central ellipse with major and minor axes of 1.5 cm and 1 cm,

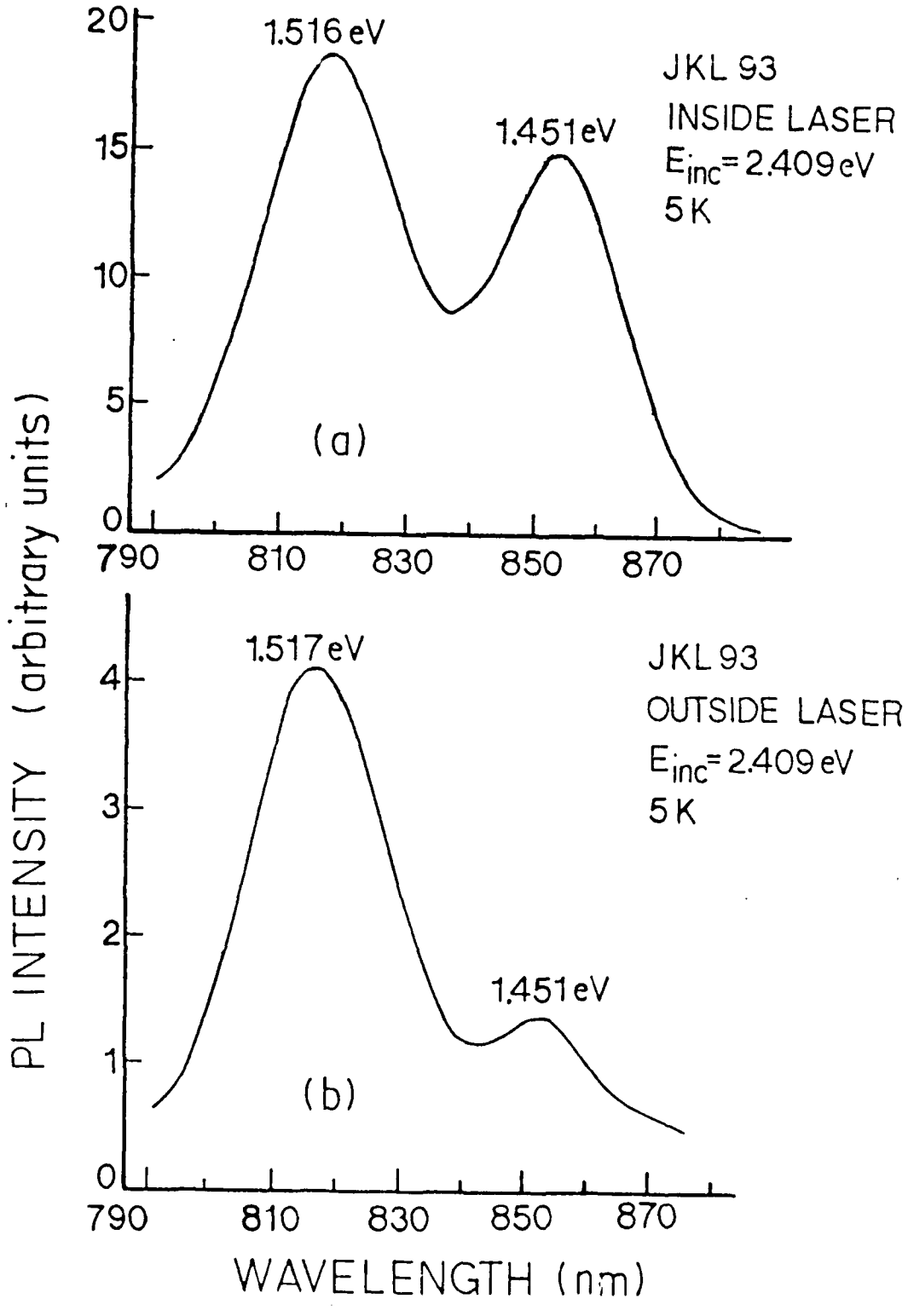
1.516 eV
1.451 eV
JKL 93
INSIDE LASER
E_inc = 2.409 eV
5 K
(a)
1.517 eV
1.451 eV
JKL 93
OUTSIDE LASER
E_inc = 2.409 eV
5 K
(b)
PL INTENSITY (arbitrary units)
WAVELENGTH (nm)
790
810
830
850
870

Fig. 19

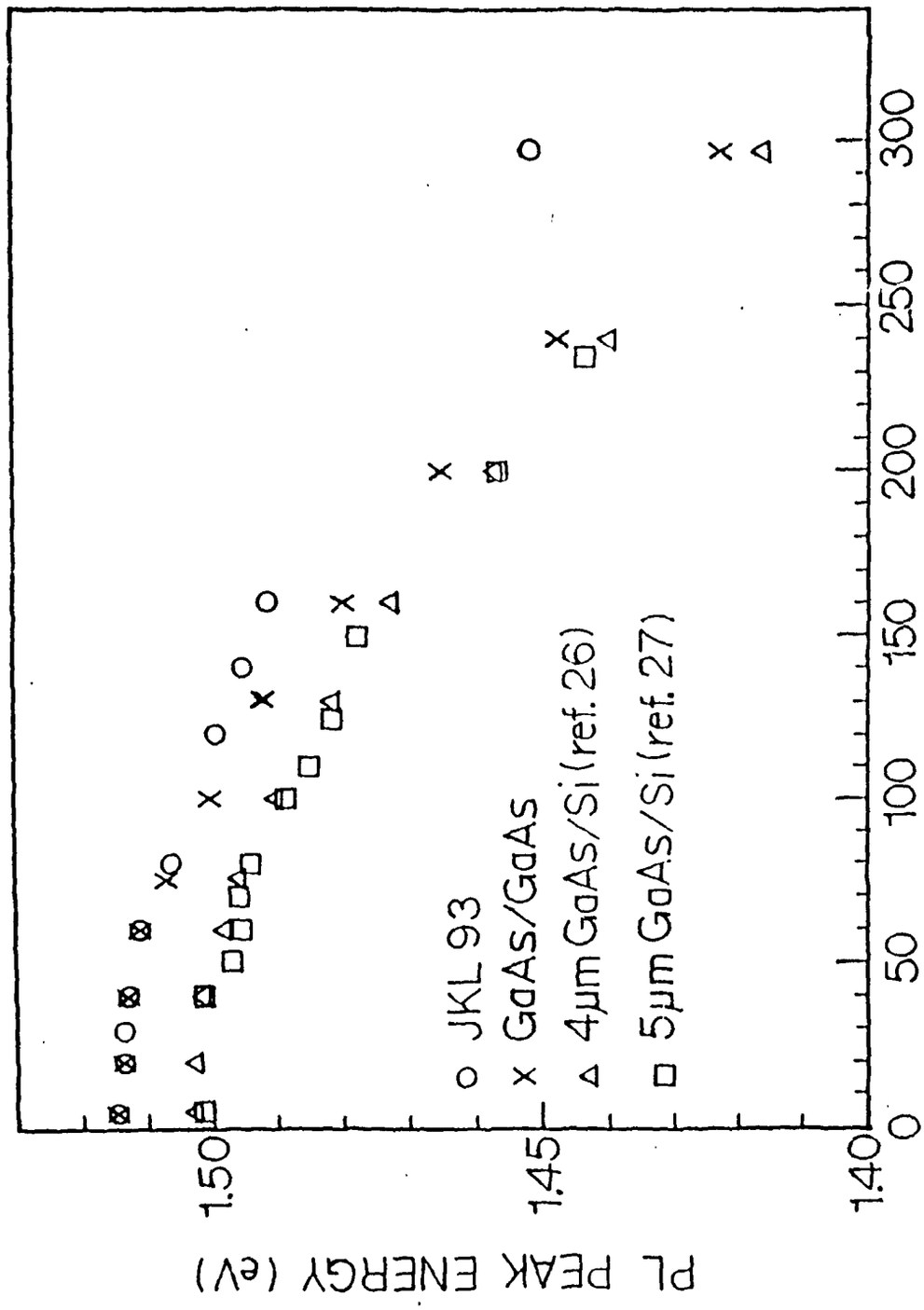
PL PEAK ENERGY (eV)
1.50
1.45
1.40
0
50
100
150
200
250
300
TEMPERATURE (K)
JKL 93
GaAs/GaAs
4μm GaAs/Si (ref. 26)
5μm GaAs/Si (ref. 27)

Fig. 20

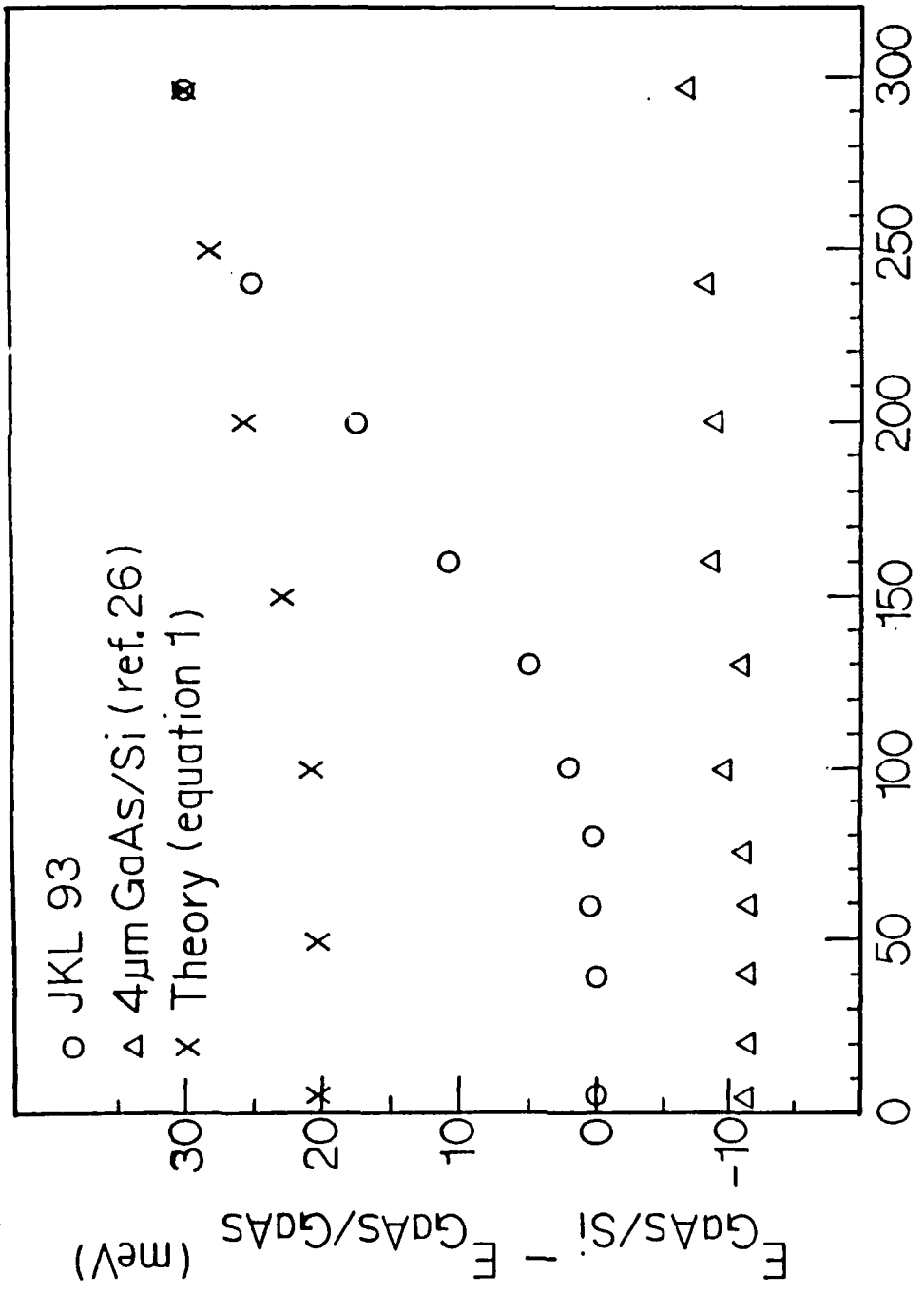
o JKL 93
Δ 4μm GaAs/Si (ref. 26)
x Theory (equation 1)
30
20
10
0
-10
0
50
100
150
200
250
300
TEMPERATURE (K)
$E_{GaAs/Si} - E_{GaAs/GaAs}$ (meV)

Fig. 21

respectively, is the laser-assisted growth area. Thus, on the same sample we can examine laser assisted and non-laser assisted (i.e. usual) growth regions for a comparative study of the optical and structural properties.

The optical properties were examined under the present grant employing PL, Raman scattering, and Rayleigh scattering. In fig. 19 are shown the 4K PL spectra from the laser assisted (panel a) and non-laser assisted (panel b) regions. Note that both regions show significant near edge luminescence (bulk GaAs excitonic luminescence being at 1.579 eV) which is at least two orders of magnitude higher than previous reports for even thick GaAs films on Si. In addition, the luminescence from the laser assisted area is about a factor of 5 higher than the non-laser assisted area, although a factor of two enhancement is a consequence of a higher film thickness. Consequently, a factor of 2 enhancement in the PL intensity from the laser assisted area is extracted from the new data. In fig. 20 and fig. 21 are shown, respectively, the temperature dependence of the PL emission peak energy and of the separation of the peak from bulk GaAs emission line. For comparison are also shown previously reported data for thick (>1 μm) GaAs films grown on Si. Though the data in figs. 20 and 21 are for the laser-assisted area, the non-laser assisted area show precisely the same values. The significant and new finding here is that figs. 20 and 21 reveal the presence of residual compressive strain in the thin film even though its thickness is more than an order of magnitude higher than predicted by the usually employed thermodynamic ground state theories. Thus the misfit dislocations present do not cause complete relaxation of the compressive strain.

Though not a part of the study undertaken under the present ARO grant, in fig. 22 we show cross sectional TEM micrographs of the laser-irradiated region which shed light on the

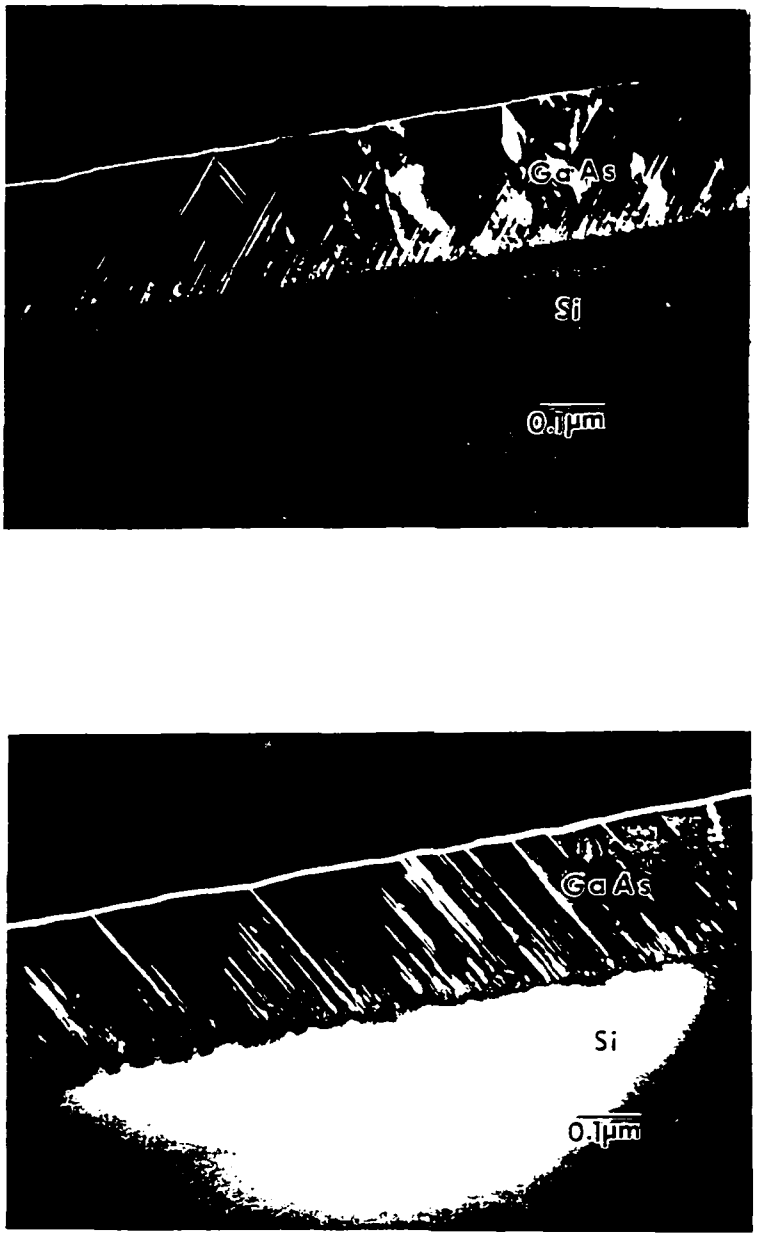

Fig. 22 Shows cross-sectional TEM Dark Field images of the two twin variants in thin (2800 A) GaAs film on Si (100) cut 4° towards [110]. Note that one type of twin reaches the surface more so than the other.

above noted inferences derived from the optical studies. The two micrographs are taken to show the existence of two types of twins of which one type dominates the surface region. We have identified this twin variant to correspond to twins that are oriented in a direction away from the step edges of the vicinal Si(100) substrate and provided energy consideration arguments to explain their origin. This is also the first time that the existence of the two twin variants, their orientational relationship to the step edges of the vicinal substrates commonly employed (to reduce the density of antiphase domain boundaries), and an explanation of their origin has been shown. Further details may be found in **publication nos. 14 and 17**.

(I.4) STRUCTURES GROWN ON PRE-PATTERNED GaAs(100) SUBSTRATES: LATERAL CONFINEMENT

Patterning of grown quantum well structures is almost invariably done to create an array of discrete devices. In recent times, such patterning is often done employing electron beam lithography motivated by the desire to create device dimensions near 0.1 μm or, from a basic physics study perspective, to create nanostructures for examination of electrical and optical properties of structures having 2 degrees of confinement (QUANTUM WIRES) or 3 degrees of confinement (QUANTUM BOXES or DOTS). An alternative to post-growth patterning, however, is to pattern the starting substrate and then grow the desired combination of ultra-thin layers. This is a particularly desirable goal for nanostructures since it affords the possibility of reducing many processing-step related introduction of defects, contaminants, etc. and, if done via a direct-write patterning technique, is compatible with in-situ patterning in an ultra-pure environment and direct transfer to the growth chamber. For an MBE system this would be a UHV environment throughout.

Under the present ARO grant we undertook optical studies of GaAs/$Al_xGa_{1-x}As$ quantum well structures grown in our MBE systems on GaAs(100) substrates patterned ex-situ via optical lithography. The growth per se is supported by the AFOSR. Although ex-situ optical patterning available to us at USC placed a lower limit of 1 μm on the dimensions of the as-patterned features (grooves, mesas, etc.), an illustrative example of a set of parallel grooves running along the [110] direction being shown in the SEM picture of fig. 23(a), through exploitation of growth kinetics we developed a unique way of creating structures down to 1000A feature size. First we provide a very brief report on the formation of quantum well structures with lateral dimensions > 2 μm.

(I.4.A) PL BEHAVIOR OF GaAs/AlGaAs WELLS:

In fig. 23(b) is shown a cross sectional TEM low magnification view of the profile GaAs/$Al_xGa_{1-x}As$ multilayered structure which has been grown on the patterned substrate of panel (a). Note the presence of facets such as (311) between the starting (111) side wall and the top (100) terrace, and (811) between the (111) side wall and the trench bottom (100) plane. In panel (c) is shown the dark-field image contrast of the trench bottom and side wall region, the lighter layers being AlGaAs. The layers defining the quantum wells on the side walls are significantly thinner than expected on the basis of the incident flux whereas the layers defining the QW's on the trench bottom are significantly thicker. This is a consequence of the inter-facet migration from the side walls to the trench bottom, a phenomenon observed in the very first studies[4] by Tsang and Cho over a decade ago. In recent times this has been exploited[5,6] to create laterally confined laser structures by exploiting the mismatch in the confined electronic states of the side wall QW's and the trench bottom QW's. In panel (d)

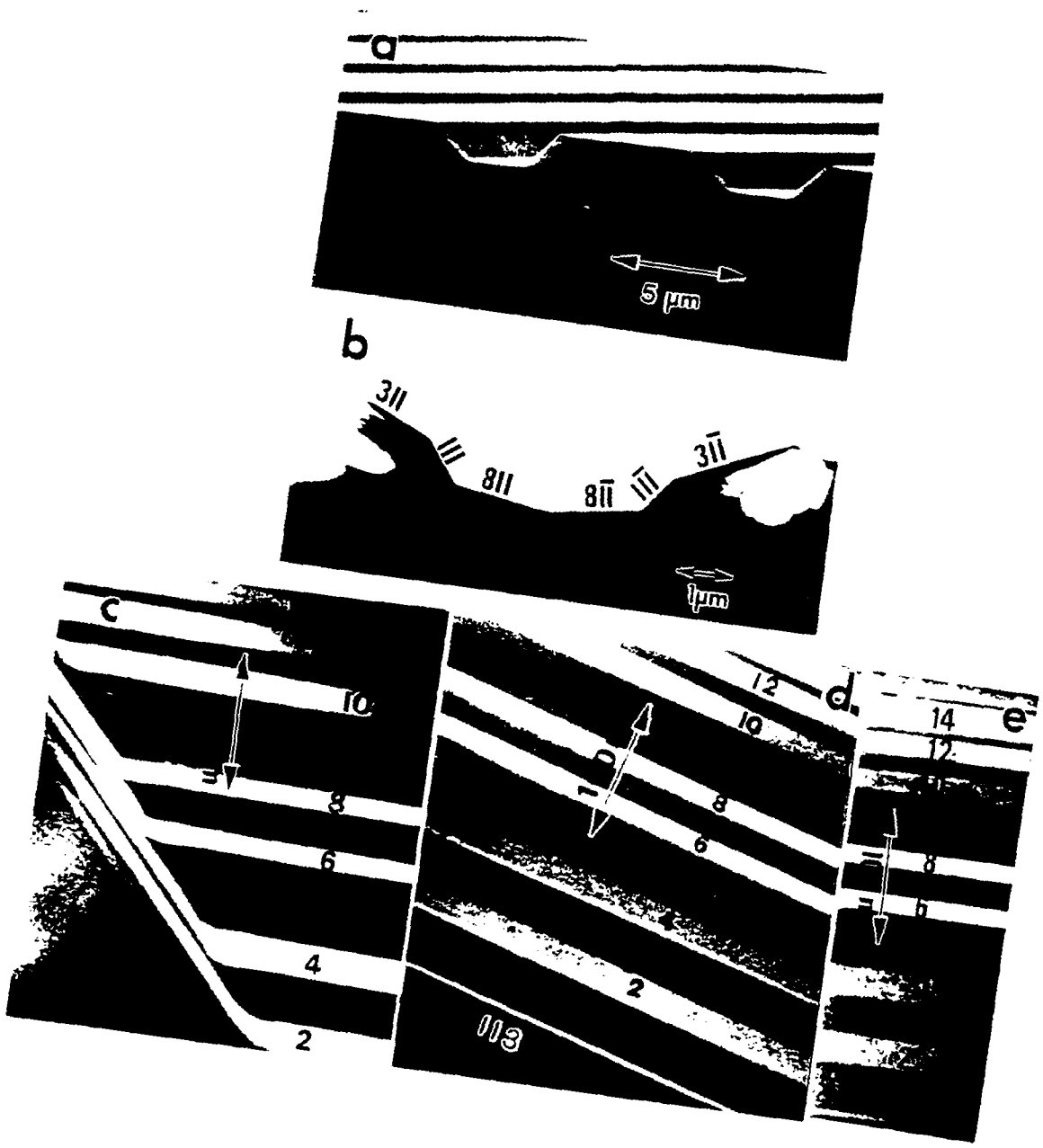
a
5 μm
b
3̄1̄1
1̄1̄1
8̄1̄1
8̄11
1̄11
3̄11
1μm
c
10
8
6
4
2
d
12
10
8
6
2
113
e
14
12
8
6

Fig. 23

is shown the QW's formed on the (311) facet. Note that, as expected from the incident flux relationship between (311), (111) and (100), the layer thicknesses in this case are intermediate between those on the (111) and (100) trench bottom. Finally, note the sharpness of the interfaces on the (311) and (100) trench bottom, indicating fairly high quality MQW formation. Panel (e) of fig. 23 shows the layer thickness in a non-patterned part of the same substrate and provides an unambiguous reference for measuring deviations in thicknesses of the layers on different facets in the patterned region.

We have examined the photoluminescence behavior of QW's grown on a variety of patterned substrates with varying groove dimensions and widths of the top (100) terrace. An illustrative result, taken on the sample of fig. 23, is shown in fig. 24. The solid curves are the PL emission from the non-patterned region and provide a marker for the optical behavior. The broken line curves show the PL emission from the uppermost three quantum wells of thickness 10 ML, 20 ML, and 40 ML in the patterned region. Note that instead of the single line emission of the non-patterned region the patterned region shows at least two peaks, one at a lower and the other at a higher energy. This is consistent with the higher than reference thickness for the QW's formed at the trench bottom (100) face and lower than reference thickness for the QW's formed on the (311) and (111) facets. The measured peak positions of the doublets do not exactly coincide with those calculated on the basis of the change in the GaAs well layer thickness alone. This we believe is as should be expected on the basis of the growth kinetics, the difference in the Ga and Al interfacet migration kinetics leading to a difference in the Al concentration of the trench bottom alloy barrier layers as compared to the ones on the side facets - lower overall Al concentration for the former and higher overall Al concentration for the latter. In addition, a fundamental feature never established in the

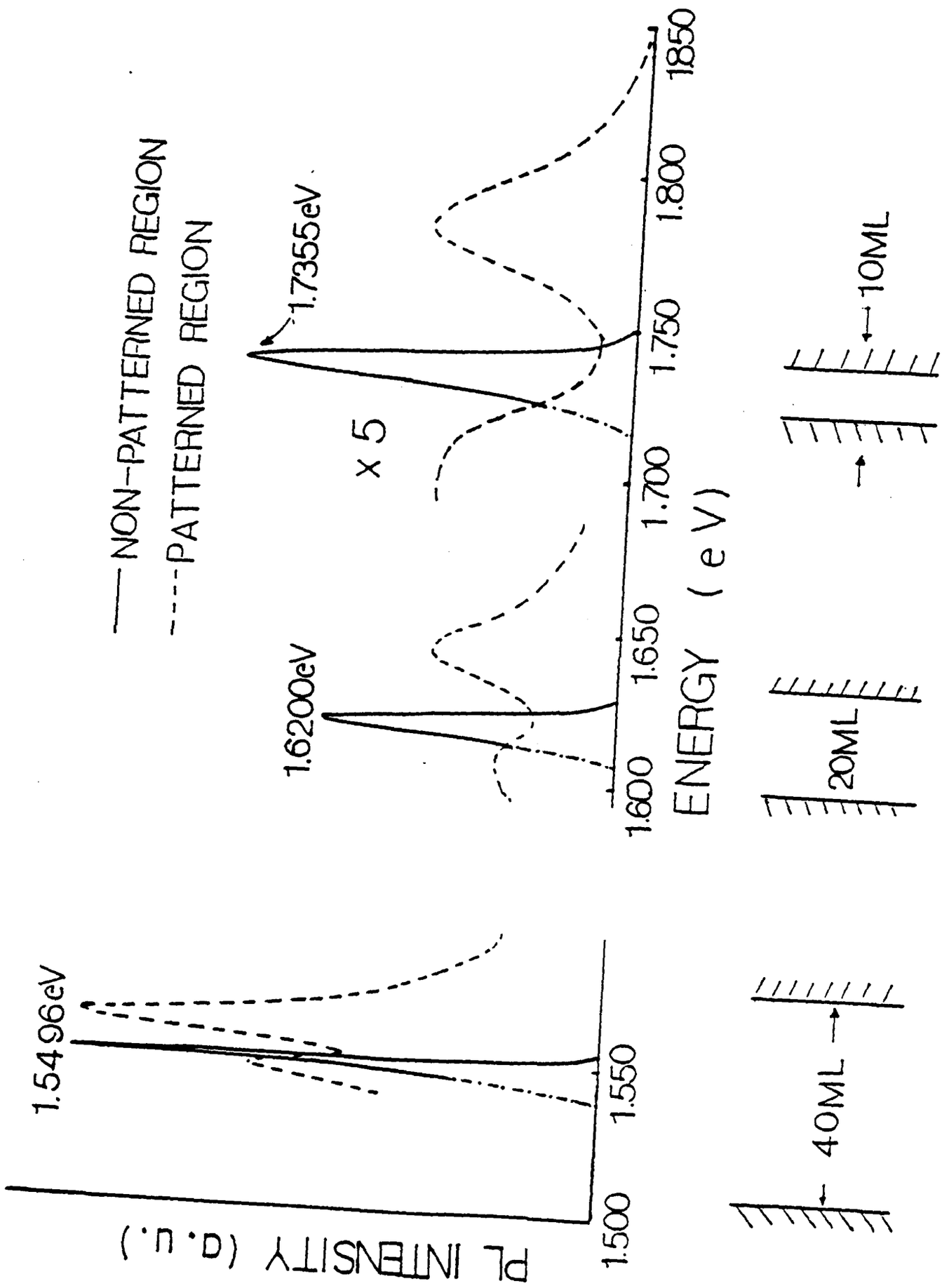
NON-PATTERNED REGION
PATTERNED REGION
1.7355eV
1.6200eV
x 5
1.600
1.650
1.700
1.750
1.800
1850
ENERGY (eV)
10ML
20ML
40ML
1.5496eV
1.500
1.550
PL INTENSITY (a.u.)

Fig. 24

literature but often assumed is the orientation dependence of the band edge discontinuity. There is no a priori reason to assume that the near 60:40 split in the band gap difference for conduction and valence bands now well tested for the (100) orientation GaAs/$Al_xGa_{1-x}As$ is also necessarily true for other orientations such as the (311) and (111) orientations involved here. Thus the precise depth of the QW potential on different facets remains uncertain.

(I.4.B) LATERALLY CONFINED STRUCTURES: IN SITU FABRICATION:

A unique and novel way of realizing laterally confined structures purely via in-situ control of growth was introduced by taking advantage of the shrinking terrace (i.e. mesa) width with growth under appropriate conditions. We briefly note two illustrative examples.

In fig. 25 is shown a dark field TEM image of a single GaAs/AlGaAs quantum well grown on a terrace of width about 4800A achieved via GaAs growth on starting mesas of width ~3 μm obtained through photolithography. Figure 26 shows the perpendicular (broken curve) and parallel (solid curve) polarized PL behavior of such a well, along with reference spectra (dash-dot curve) obtained from the non-patterned regions of the same wafer. The three emission peaks in the Pl from the patterned region correspond to the quantum wells on the top terrace (1.563eV peak), on the trench bottom (1.611 eV peak), and on the side walls (1.712 eV). Note the strong polarization dependence (9.6%) of the emission at 1.563 eV from the top terrace quantum well indicating the presence of lateral confinement on optical properties. As a further check, selective etching was used to remove only the top terrace quantum well region and the PL behavior again examined. Only the 1.563 eV peak was found to be absent, reconfirming that the polarization dependence of the PL is a true lateral confinement effect. Another consequence of this lateral confinement, namely enhancement of

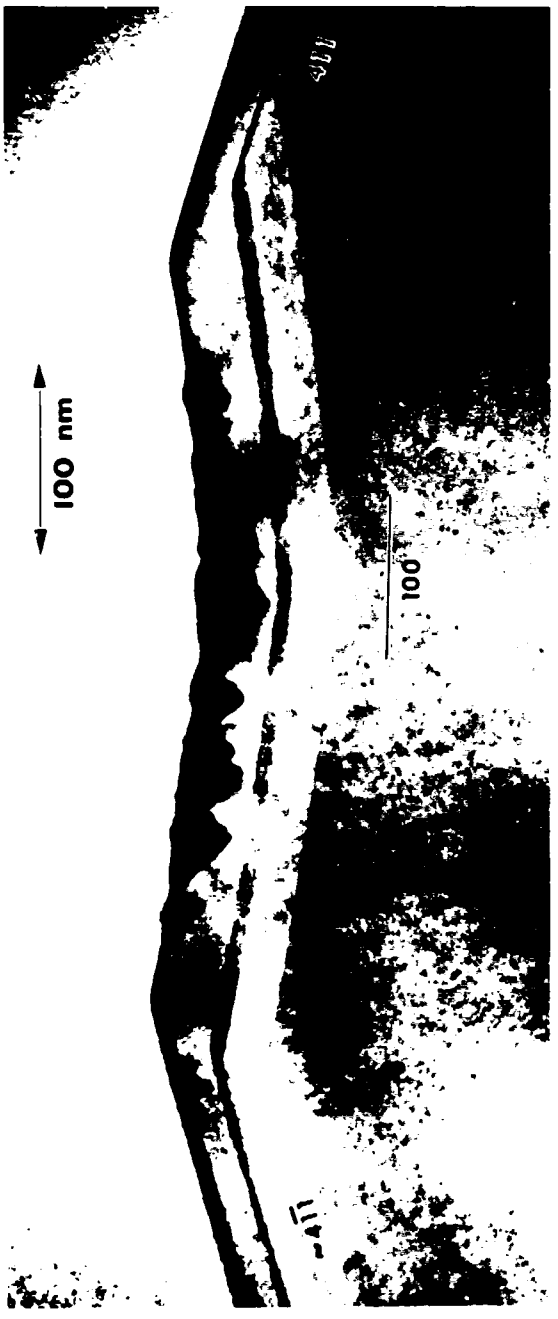

Fig. 25

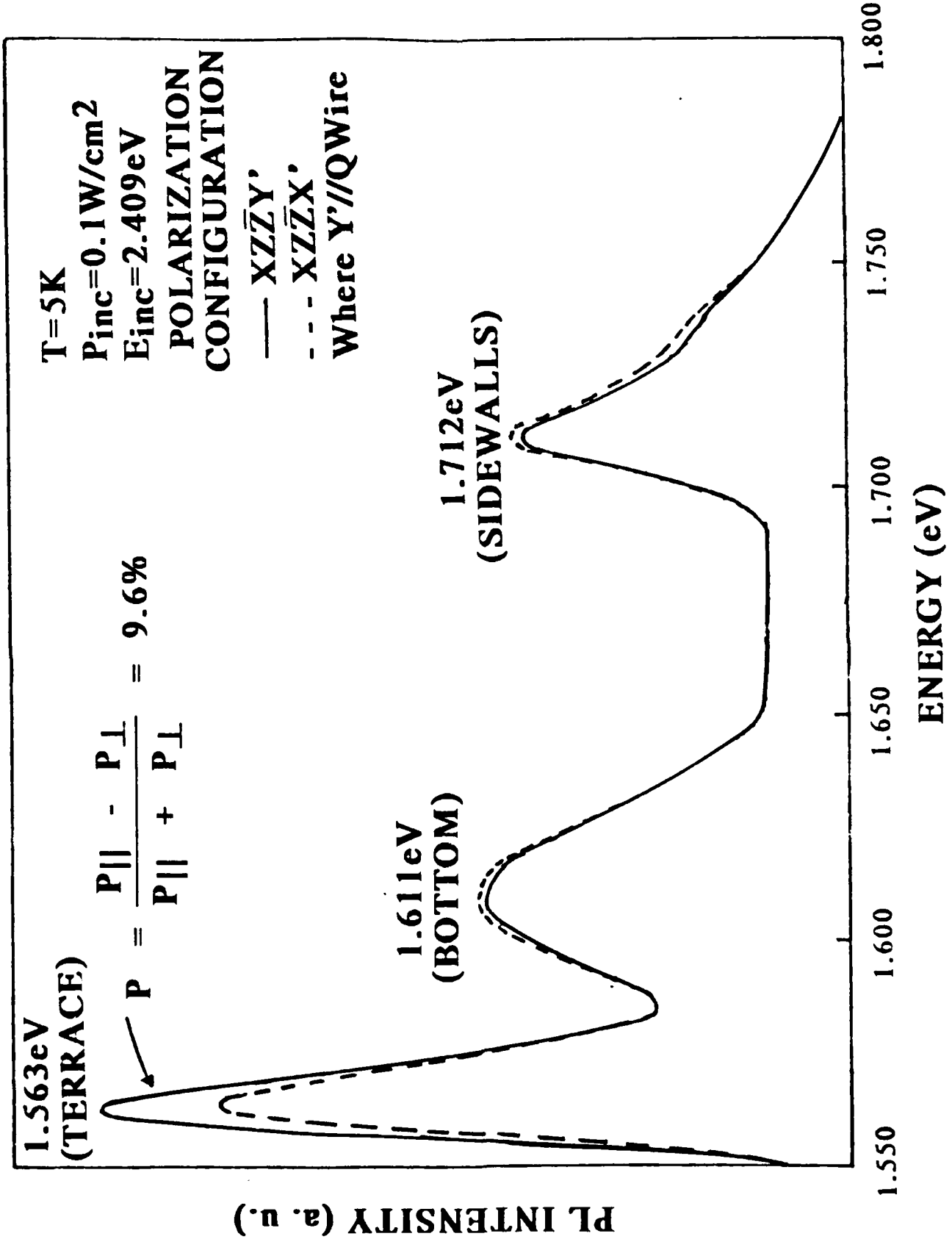
T=5K
Pinc=0.1W/cm2
Einc=2.409eV
POLARIZATION CONFIGURATION
—— XZZ̄Y'
- - - XZZ̄X'
Where Y'//QWire
1.563eV (TERRACE)
P = (P|| - P⊥) / (P|| + P⊥) = 9.6%
1.611eV (BOTTOM)
1.712eV (SIDEWALLS)
1.550
1.600
1.650
1.700
1.750
1.800
ENERGY (eV)
PL INTENSITY (a. u.)

Fig. 26

the oscillator strength beyond that achieved in a quasi-two dimensional well, is manifest in the fact that the PL signal from the top terraces of the patterned region is the strongest even though the area covered is only ~4% of the total patterned area. To examine this further, the incident photon energy was varied from higher (fig. 27a) to lower (fig. 27b) than the lowest transition energy of the sidewall quantum well. A slight increase, rather than a drastic decrease, in the Pl signal from the top terrace quantum wells was observed, indicating that carrier drift from the sidewall quantum wells into the top terrace quantum wells is not a contributing factor to the strong PL signal from the latter. Rather, it is a true consequence of the lateral confinement achieved on the length scale of ~4800A. Details may be found in **publication no. 16.**

IN SITU FABRICATED QUANTUM WIRE STRUCTURES:

Finally, in fig. 28 we show an example of a remarkable way of exploiting growth kinetics for in-situ creation of quantum wires and quantum dots, even though patterning may be done ex-situ and on length scales of > 1 μm. Under appropriate growth conditions, the starting sharp edge between the top (100) terrace and the (111) side wall of the as-patterned substrate (shown in the inset) gives rise to the formation of a (311) transition facet immediately after thermal desorption of the native oxide prior to growth initiation. This is clearly seen in the main figure where the very first light colored "line" corresponds to 10 ML AlAs layer grown as a marker to define the starting profile of the substrate after oxide desorption. Note that during subsequent deposition of GaAs, no growth occurs on the (311) facet so long as the top(100) terrace remains adjacent. The $Al_{0.4}Ga_{0.6}As$ marker layer numbered 2 not only clearly demonstrates this behavior, but also then shows that the truncated pyramidal

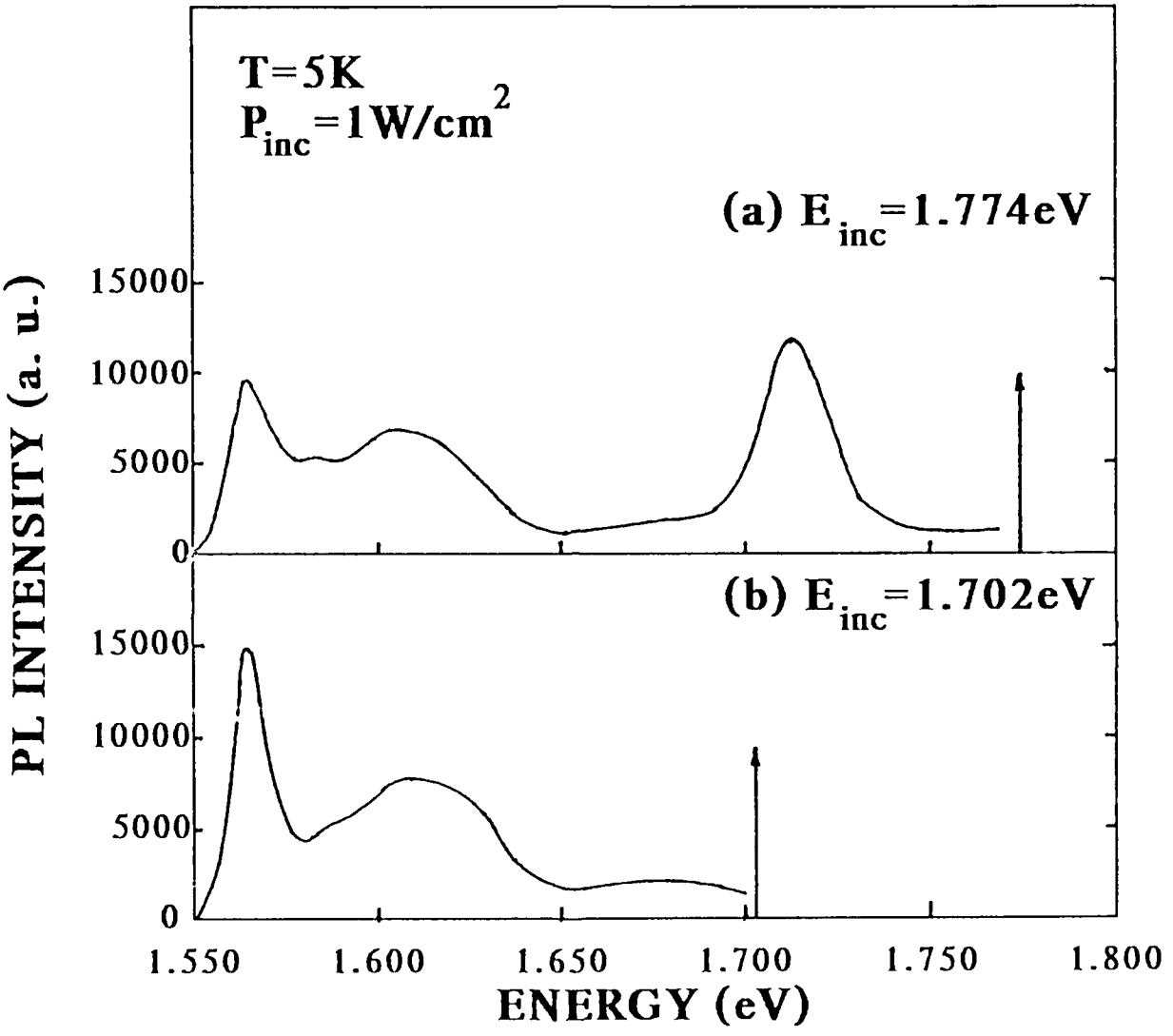
T=5K
P_inc=1W/cm^2
(a) E_inc=1.774eV
(b) E_inc=1.702eV
PL INTENSITY (a. u.)
15000
10000
5000
0
1.550
1.600
1.650
1.700
1.750
1.800
ENERGY (eV)

Fig. 27

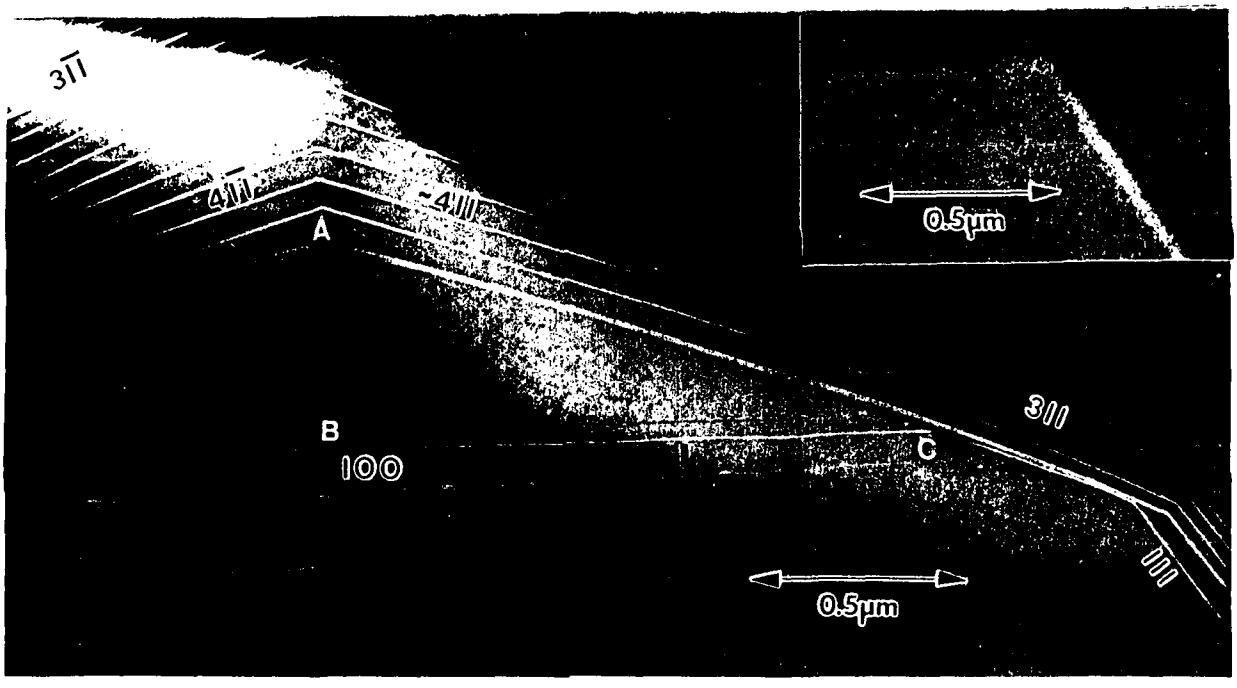

Fig. 28

profile of the GaAs growing on the top (100) terrace provides a (100) "substrate" of smaller and smaller lateral dimension with growth. The lateral dimension defined by the marker layer 2 in the region labelled A in fig. 28 is about 2000 A. Subsequent growth of GaAs and deposition of the $Al_{0.4}Ga_{0.6}As$ layer labelled 3 then creates, in-situ, a pyramidal shaped quantum wire structure. This is a powerful way of creating nanostructures for a variety of basic optical and electrical studies for it avoids a number of contamination and damage issues faced with in techniques employing patterning on the scale of the desired nanostructure. It also has the great practical advantage that it makes possible creation of at least certain types of nanostructures without the need for elaborate and expensive ex-situ or in-situ patterning and processing techniques (such as electron beam lithography and focussed ion beam induced impurity disordering being employed in the few attempts at producing nanostructures reported so far). The result shown in fig.28 is the first demonstration of in-situ fabrication of a nanostructure and **was reported in publication no.23.**

REFERENCES:

1. A. Ourzmad, paper presented at the MRS Fall Meeting, (Boston, Ma.) Dec. 1988.

2. A. Madhukar and S. Das Sarma, Surf. Sc. 98, 135 (1980); S. Das Sarma and A. Madhukar, Phys. Rev. B22, 2823 (1980).

3. D.A. B. Miller, D.S. Chemla, T.C. Damen, T.H. Wood, C.A. Burras Jr., A.C. Gossard and W. Weigmann, IEEE Jour. Quantum Elec. QE-21, 1462 (1985) and references therein.

4. W.T. Tsang and A.Y.Cho, App. Phys. Letts. 30, 293 (1977).

5. E. Kapon, M.C. Tamargo and D.M. Hwang, App. Phys. Lett. 50, 347 (1987).

6. E. Kapon, C.P. Yun, D.M. Hwang, M.C. Tamargo, J.P. Harbison and R. Bhat, Proceedings of the SPIE Symposium on "Growth of Advanced Compound Semiconductor Structures, Editor A. Madhukar, Vol.944, p.80 (1988).

II. ARO SUPPORTED PUBLICATIONS:

1. S.B. Ogale, A. Madhukar, F. Voillot, M. Thomsen, W.C. Tang, T.C. Lee, J.Y. Kim and P. Chen, "Atomistic Nature of Heterointerfaces in III-V Semiconductor-Based Quantum-Well Structures and its Consequences for Photoluminescence Behavior", Phys. Rev. B36, 1662 (1987).

2. S.B. Ogale, A. Madhukar and N.M. Cho, "Photoluminescence Linewidth Systematics for Semiconductor Quantum Well Structures with Graded Interface Composition Profile", App. Phys. Letts. 63, 578 (1987).

3. S.B. Ogale, A. Madhukar and N.M. Cho, "Influence of Transverse Electric Field on the Photoluminescence Linewidth of Excitonic Transition in Quantum Wells: Alloy Disorder and Composition Fluctuation Contributions", J. Appl. Phys. 62, 1381 (1987).

4. N.M. Cho, S.B. Ogale and A. Madhukar, "Low Temperature Electron Transport in One-side-modulation-doped $Al_{0.33}Ga_{0.67}As/GaAs/Al_{0.33}Ga_{0.67}As$ Single Quantum Well Structure", Appl. Phys. Lett. 51, 1016 (1987).

5. N.M. Cho, S.B. Ogale and A. Madhukar, "Electron Transport in One-side-modulation-doped Single Quantum Well Structure: Remote Ion Scattering Contribution", Phys. Rev. B36, 6472 (1987).

6. Madhukar, P.D. Lao, W.C. Tang, M. Aidan and F. Voillot, "Observation of Phonon Modes through Resonant Mixing with Electronic States in the Secondary Emission Spectra of $GaAs/Al_{0.32}Ga_{0.68}As$ Single Quantum Well", Phys. Rev. Lett. 59, 1313 (1987).

7. P.D. Lao, W.C. Tang, A. Madhukar and F. Voillot, "Resonant Mixing between Electronic and Optical Vibrational States of a Quantum Well Structure", Jour. de Physique, 48, C5-121 (1987).

8. W.C. Tang, P.D. Lao, A. Madhukar and N.M. Cho, "A Combined Rayleigh and Raman scattering study of $Al_xGa_{1-x}As$ Grown via Molecular Beam Epitaxy Under Reflection High Energy Electron Diffraction Determined Growth Conditions", Appl. Phys. Lett.52, 42 (1988).

9. Anupam Madhukar, "Exploiting Kinetics in Molecular Beam Epitaxial Growth for Realization of High Quality Normal and Inverted Interfaces", Workshop on HEMT, Organized by U.S. Army Electronics and Device Technology Laboratory, Ft. Monmouth, New Jersey, Jan, 27-28, 1988.

10. P.G. Newman, N.M.Cho, D.J.Kim, A.Madhukar, D.D.Smith, T.R.Aucoin and G.J.Iafrate, "Surface Kinetic Considerations for MBE Growth of High Quality Inverted Heterointerfaces", Proceedings of the 15th PCSI Conference, (Feb. 1-4, 1988; Asilomar, Ca.); Jour. Vac. Sc. Tech.B6, 1483 (1988).

11. N.M. Cho, P.G. Newman, D.J.Kim, A. Madhukar, D.D. Smith, T. Aucoin and G.J.

Iafrate, "Realization of High Mobility in Inverted $Al_xGa_{1-x}As$/GaAs Heterojunctions", App. Phys. Lett. 52, 2037 (1988).

12. Pudong Lao, Wade C. Tang, A. Madhukar and P. Chen, "Alloy Disorder Effects in Molecular Beam Epitaxically Grown $Al_xGa_{1-x}As$ Examined Via Raman and Rayleigh Scattering and near Edge Luminescence", Proceedings of the SPIE Conference on "Advances in Semiconductors and Superconductors: Physics and Device Applications" (13-18 March, 1988, Newport Beach Mariott Hotel, CA), SPIE Vol. 946, p.150 (1988).

13. W.C. Tang, Pudong Lao, and A. Madhukar, "Optical Investigation of Resonant Mixing Between Electronic and Optical Vibrational Levels in GaAs/$Al_xGa_{1-x}As$ Single Quantum Wells", Proceedings of the SPIE Conference on "Advances in Semiconductors and Superconductors; Physics and Device Applications", (13-18 March, 1988, Newport Beach Mariott Hotel, CA), SPIE Vol. 943, p.170 (1988).

14. F.J. Grunthaner, A. Madhukar, J.K. Liu, W.C. Tang, P.D. Lao, S. Guha, P. Anderson, J. Ionelli and B. Pate, "Laser-assis-ted Molecular Beam Epitaxial Growth of GaAs on Si(100)", SPIE Proceedings, Vol. 944, 153 (1988).

15. Pudong Lao, Wade C. Tang, A. Madhukar and P. Chen, "A Combined Single Phonon Raman and Photoluminescence Study of Direct and Indirect Band Gap $Al_xGa_{1-x}As$ Alloys Grown by Molecular Beam Epitaxy", Jour. Appl. Phys. 65, 1676 (1989).

16. S. Guha, A. Madhukar, K. Kaviani, Li Chen, R. Kuchibhotla, R. Kapre, M. Hyugaji, and Z. Xie, "Molecular Beam Epitaxical Growth of $Al_xGa_{1-x}As$ on non-planar Patterned GaAs (100)", MRS Proceedings Vol. 145, p.27 (1989).

17. P.D. Lao, W.C. Tang, K.C. Rajkumar, S. Guha, A. Madhukar, J.K. Liu and F.J. Grunthaner, "Some Optical and Electron Microscope Comparative Studies of Excimer Laser Assisted and Non-Assisted Molecular Beam Epitaxically Grown Thin GaAs Films on Si" Jour. App. Phys. 67, 6445 (1990).

18. D.J. Kim, A. Madhukar, K.Z. Hu, W. Chen, "Realization of High Mobilities at Ultra Low Electron Density in GaAs/$Al_{0.3}Ga_{0.7}As$ Inverted Heterojunctions", App. Phys. Lett. 56, 1874 (1990).

19. Kezhong Hu, P.M. Echternach, A. Madhukar, H.M. Bozler and C.R. Stapleton, "Magneto-transport Behavior of High Mobility Inverted GaAs/AlGaAs Heterostructures at Ultralow Electron Density", Phys. Rev. B (Submitted).

20. R. Kapre, A. Madhukar, K. Kaviani, S. Guha and K.C.Rajkumar, "Realization and Analysis of GaAs/AlAs/$In_{0.1}Ga_{0.9}As$ Based Resonant Tunneling Diodes with High Peak to Valley Ratios at Room Temperature, App. Phys. Lett. 56, 922 (1990).

21. R. Kapre, A. Madhukar and S. Guha, "$In_{0.25}Ga_{0.75}As$/AlAs Based Resonant Tunneling Diodes Grown on Pre-patterned and Non-patterned GaAs(100) Substrates, IEEE Electron Device Lett, 11, 270 (1990).

22. K. Pastor, J. Leotin and A. Madhukar, Proceedings of the 20th International Conference of the Physics of Semiconductors, Tessaloniki, Greece, Aug. 1990 (To be Published).

23. A. Madhukar, "The Nature of Molecular Beam Epitaxy and Consequences for Quantum Microstructures" in Topics in Applied Physics, Entitled "Physics of Quantum Electron Devices" (Ed. F. Capasso), Springer Publications, p.13 (1990).

CONFERENCE PRESENTATIONS:

1. P.D. Lao, W.C. Tang, A. Madhukar and F. Voillot, "Resonant Mixing between Electronic and Optical Vibrational States of a Quantum Well Structure", 3rd International Conference on Modulated Semiconductor Structures (July 1987, Montpelier, France).

2. F.J. Grunthaner, A. Madhukar, J.K. Liu, W.C. Tang, P.D. Lao, S. Guha, P. Anderson, J. Ionelli and B. Pate, "Laser-assis-ted Molecular Beam Epitaxial Growth of GaAs on Si(100)", 15th PCSI Conference, (Feb. 1-4, 1988; Asilomar, Ca.).

3. Pudong Lao, Wade C. Tang, A. Madhukar and P. Chen, "Alloy Disorder Effects in Molecular Beam Epitaxically Grown $Al_xGa_{1-x}As$ Examined Via Raman and Rayleigh Scattering and near Edge Luminescence", SPIE Conference on "Advances in Semiconductors and Superconductors: Physics and Device Applications" (13-18 March, 1988, Newport Beach Mariott Hotel, CA).

4. W.C. Tang, Pudong Lao, and A. Madhukar, "Optical Investigation of Resonant Mixing Between Electronic and Optical Vibrational Levels in $GaAs/Al_xGa_{1-x}As$ Single Quantum Wells", SPIE Conference on "Advances in Semiconductors and Superconductors; Physics and Device Applications", (13-18 March, 1988, Newport Beach Mariott Hotel, CA).

III. STUDENTS/POST-DOCS TRAINED:

1. Mr. Nam-Min Cho (Ph.D. Oct. 1988)

2. Mr. Roger Kuroda (Ph.D. Expected 1990)

3. Mr. Do-Jin Kim (Ph.D. Oct. 1989)

4. Mr. Wade C. Tang (Ph.D. Dec. 1989)

5. Mr. R. Kapre (Ph.D. Expected Dec. 1990)

6. Mr. Kezhong Hu (Ph.D. Expected 1991)

7. Dr. P.D. Lao (July '86 - Aug. '88)

8. Dr. S. Xie (Jan. '88 - Dec. '88).

IV. COLLABORATIONS/INTERACTIONS:

During the course of the activities undertaken under the present ARO grant a number of fruitful collaborations/interac-tions with colleagues at USC and other institutions emerged. These collaborations served the purpose of bringing complimentary expertise and/or facilities to bear upon issues of mutual interest and thus leverage each other's resources and investments. The dominant collaborations/interactions are noted below;

1. Profs. A.R. Tanguay Jr. and K. Jenkins (USC):

   Collaborative work on realization of 2D arrays of SLM structures for implementation of neural network models. Prof. Jenkins provides the systems perspective and Prof. Tanguay device processing and testing efforts.

2. Drs. D.D. Smith, M. Cole and M. Dutta (U.S. Army Electronic and Devices Laboratory, Ft. Monmouth, N.J.):

   The collaborative efforts here which bring complimentary expertise and resources to bear upon problems of common interest are;

   (a) Magneto-quantum transport (Dr. D.D. Smith)

   (b) High Resolution Electron Microscopy, including image simulation (Dr. M. Cole).

   (c) Micro-Raman Scattering studies of the laterally confined structures (Dr. M. Dutta)

3. Prof. J. Leotin (INSA, Toulouse, France):

   Collaborative work with Prof. Leotin utilizing the high magnetic field (up to 60T) and far infrared cyclotron resonance facilities.